

1 The effects of multidimensional drought on land cover change and
2 vegetation productivity in continental Chile

3 Francisco Zambrano^{a,1,*}, Anton Vrieling^b, Francisco Meza, Iongel Duran-Llacer, Francisco Fernández^c,
4 Alejandro Venegas-González, Nicolas Raab, Dylan Craven

^a Universidad Mayor, Hémera Centro de Observación de la Tierra, Facultad de Ciencias, Escuela de Ingeniería en Medio Ambiente y Sustentabilidad, Santiago, Chile, 7500994

^b University of Twente, Faculty of Geo-Information Science and Earth Observation (ITC), Enschede, The Netherlands,

^c Universidad San Sebastián,

5 **Abstract**

The north-central region of Chile has been the focus of research studies due to the persistent decrease in water supply, which is impacting the hydrological system and vegetation development. This persistent period of water scarcity has been defined as a megadrought. The aim of our study is to evaluate the land cover change over continental Chile and to examine how this is connected to drought indices of water supply, atmospheric evaporative demand (AED), soil moisture, and their effects on vegetation productivity. The drought indices were derived using monthly ERA5-Land reanalysis data spanning from 1981 to 2023. The Moderate-Resolution Imaging Spectroradiometer (MODIS) datasets were utilized to obtain information on annual land cover and monthly vegetation productivity. We analyzed short- (1, 3, 6 months) to long-term (12, 24, 36 months) time scales of drought. Our results showed that land cover change was highest in the south-central part of the country, reaching changes as high as 36% in the surface type. The water demand has increased for the whole country, with a major increase in the north. The AED and soil moisture evidence a decreasing trend, which decreases at longer time scales and from north to south. The extreme south part of the country shows an increase in supply. Vegetation productivity has a negative trend in the north-central region for all land cover types. On the other hand, forests seem to be the most resistant type to drought. The types that show to be most affected by variation in climate conditions are shrublands, savannas, and croplands. The drought indices that have the capability of explaining to a major degree the variance in vegetation productivity are the ones that consider soil moisture for twelve months and the combined effect of precipitation and AED for 24 and 12 months. The results indicate that the north-central region is the most sensitive to water supply deficits lasting longer than a year.

6 **Keywords:** drought, land cover change, satellite

7 **1. Introduction**

8 Drought is often classified as meteorological when there is a decrease in precipitation below the mean
9 average of several years (more than 30 years), hydrological when these anomalies last for long periods (months
10 to years) and affect water systems, and agricultural when the deficit impacts plant health anomalies and
11 leads to decreased productivity (Wilhite and Glantz, 1985). However, it is important to note that drought

*Corresponding author

Email addresses: francisco.zambrano@umayor.cl (Francisco Zambrano), a.vrieling@utwente.nl (Anton Vrieling), francisco.fernandez@uss.cl (Francisco Fernández)

¹This is the first author footnote.

is also influenced by human activities, which were not considered in the definitions. Thus, Van Loon et al. (2016) and AghaKouchak et al. (2021) have given an updated definition of drought for the Anthropocene, suggesting that it should be considered the feedback of humans' decisions and activities that drives the anthropogenic drought. Simultaneously, drought leads to heightened tree mortality and induces alterations in land cover and land use, ultimately affecting ecosystems (Crausbay et al., 2017). Even though many ecological studies have misinterpreted how to characterize drought, for example, sometimes considering "dry" conditions as "drought" (Slette et al., 2019). Then, Crausbay et al. (2017) proposed the ecological drought definition as "an episodic deficit in water availability that drives ecosystems beyond thresholds of vulnerability, impacts ecosystem services, and triggers feedback in natural and/or human systems." In light of current global warming, it is crucial to study the interaction between drought and ecosystems in order to understand their feedback and impact on water security. (Bakker, 2012)

Human-induced greenhouse gas emissions have increased the frequency and/or intensity of drought as a result of global warming, according to the sixth assessment report (AR6) of the Intergovernmental Panel on Climate Change (IPCC) (Calvin et al., 2023). The evidence supporting this claim has been strengthened since AR5 (IPCC, 2013). Recent studies, however, have produced contrasting findings, suggesting that drought has not exhibited a significant trend over the past forty years. (Vicente-Serrano et al., 2022; Kogan et al., 2020). Vicente-Serrano et al. (2022) analyzed the meteorological drought trend on a global scale, finding that only in a few regions has there been an increase in the severity of drought. Moreover, they attribute the increase in droughts over the past forty years solely to an increase in atmospheric evaporative demand (AED), which in turn enhances vegetation water demand, with important implications for agricultural and ecological droughts. Also, they state that "the increase in hydrological droughts has been primarily observed in regions with high water demand and land cover change". Similarly, Kogan et al. (2020) analyzed the drought trend using vegetation health methods, finding that for the globe, hemispheres, and main grain-producing countries, drought has not expanded or intensified for the last 38 years. Further, the Masson-Delmotte (2021) suggests that there is a high degree of confidence that rising temperatures will increase the extent, frequency, and severity of droughts. Also, AR6 (Calvin et al., 2023) predicts that many regions of the world will experience more severe agricultural and ecological droughts even if global warming stabilizes at 1.5°–2°C. To better evaluate the impact of drought trends on ecosystems, assessments are needed that relate meteorological and soil moisture variables to their effects on vegetation.

From 1960 to 2019, land use change has impacted around one-third of the Earth's surface, which is four times more than previously thought (Winkler et al., 2021). Multiple studies aim to analyze and forecast changes in land cover globally (Winkler et al., 2021; Song et al., 2018) and regionally (Chamling and Bera, 2020; Homer et al., 2020; Yang and Huang, 2021). Some others seek to analyze the impact of land cover change on climate conditions such as temperature and precipitation (Luyssaert et al., 2014; Pitman et al., 2012). There is less research on the interaction between drought and land cover change (Chen et al., 2022; Akinyemi, 2021; Peng et al., 2017). Peng et al. (2017) conducted a worldwide investigation utilizing net primary production to examine the spatial and temporal variations in vegetation productivity at global level. The study aimed to assess the influence of drought by comparing the twelve-month Standardized Precipitation Evapotranspiration Index (SPEI) and land cover change. According to their findings, drought is responsible for 37% of the decline in vegetation productivity, while water availability accounts for 55% of the variation. Chen et al. (2022) studied the trend of vegetation greenness and productivity and its relation to meteorological drought (SPEI of twelve months in December) and soil moisture at the global level. The results showed lower correlations (<0.2) for both variables. Akinyemi (2021) evaluates drought trends and land cover change using vegetation indices in Botswana in a semi-arid climate. These studies mostly looked at how changes in land cover and vegetation productivity are related to a single drought index (SPEI) over a single time period of 12 months. SPEI takes into account the combined effect of precipitation and AED as a water balance, but it does not allow us to know the contribution of each variable on its own. Some things worth investigating in terms of land cover change and vegetation productivity are: i) How do they respond to short- to long-term meteorological droughts? ii) How do they behave in humid and arid climatic zones regarding drought? And iii) What is the role of soil moisture? Likewise, there is a lack of understanding of how the alteration in water supply and demand is affecting land cover transformations.

Chile's diverse climatic and ecosystem types (Beck et al. (2023);Luebert and Pliscoff (2022)) make it an ideal natural laboratory for studying climate and ecosystems. Additionally, the country has experienced severe drought conditions that have had significant effects on vegetation and water storage. Central Chile faced a persistent precipitation deficit between 2010 and 2022, defined as a megadrought (Garreaud et al., 2017), which has impacted the Chilean ecosystem. This megadrought was defined by the Standardized Precipitation Index (SPI) of twelve months in December having values below one standard deviation. Some studies have addressed how this drought affects single ecosystems in terms of forest development (Miranda et al., 2020; Venegas-González et al., 2018), forest fire occurrence (Urrutia-Jalabert et al., 2018), and crop productivity (Zambrano, 2023; Zambrano et al., 2018, 2016). We found one study regarding land cover and drought in Chile. The study by Fuentes et al. (2021) evaluates water scarcity and land cover change in Chile between 29° and 39° of south latitude. Fuentes et al. (2021) used the SPEI of one month for evaluating drought, which led to misleading results. For example, they did not find a temporal trend in the SPEI but found a decreasing trend in water availability and an increase trend on AED, which in turn should have been capable of being captured with longer time scales of the SPEI. The term "megadrought" in Chile is used to describe a prolonged water shortage that lasts for several years, resulting in a permanent deficit that impacts the hydrological system (Boisier et al., 2018). Hence, it is imperative to assess temporal scales that take into account the cumulative effect within some years. There is little knowledge about the relationship between drought and ecosystem in Chile; thus, it is important to understand in more detail how meteorological and soil moisture droughts influence ecosystem dynamics to inform adaptation options.

A detailed spatiotemporal assessment of the interaction of drought for short- to long-term and land cover change requires information on vegetation as well as weather variables such as precipitation, temperature, and soil moisture. Weather networks in Chile present some disadvantages, such as spatio-temporal gaps, a short history, and irregular quality, which make them difficult to represent the whole extent of the country spatially. In order to do this, we use reanalysis data from ERA5-Land (Muñoz-Sabater et al., 2021) to create drought indices that consider AED, precipitation, and soil moisture over a range of time periods, from the short to the long term. Also, we use vegetation spectral information and annual land cover change from the Moderate-Resolution Imaging Spectroradiometer (MODIS). We expect to gain insight regarding the temporal evolution of water demand, water supply, and soil moisture, as well as the interaction with land cover change and vegetation productivity. Here, we analyze the multi-dimensional impacts of drought across ecosystems in continental Chile. More specifically, we aim to assess: i) temporal changes in land-use cover and the direction and magnitude of their relationships with drought indices for water demand and supply, soil moisture, and vegetation productivity; ii) short- to long-term temporal trends in multi-scalar drought indices; and iii) the relationship between vegetation productivity and drought indices for water demand and supply and soil moisture across Chilean ecosystems.

2. Study area

Continental Chile has a diverse climate conditions with strong gradients from north to south and east to west (Aceituno et al., 2021) (Figure 1 a), which determines its great ecosystem diversity (Luebert and Pliscoff (2022)) (Figure 1 c). The Andes Mountains are a main factor in climate latitudinal variation (Garreaud, 2009). In order to characterize the climate and ecosystem of Chile, we utilize the Köppen-Geiger classification system developed by Beck et al. (2023) and the land cover data derived from the MODIS product for the period of 2001–2022, based on the International Geosphere-Biosphere Programme (IGBP) classification scheme proposed by Friedl and Sulla-Menashe (2019). “Norte Grande” and “Norte Chico” predominate in an arid desert climate with hot (Bwh) and cold (Bwk) temperatures. At the south of “Norte Chico,” the climate changes to an arid steppe with cold temperatures (Bsk). In these two northern regions, the land is mostly bare, with a minor surface of vegetation types such as shrubland and grassland. In the zones “Centro” and the north half of “Sur,” the main climate is Mediterranean, with warm to hot summers (Csa and Csb). Land cover in “Centro” comprises a significant amount of shrubland and savanna (50%), grassland (16%), forest (8%), and croplands (5%). An oceanic climate (Cfb) predominates in the south of “Sur” and the north of “Austral.” Those zones are high in forest and grassland. The southern part of

112 the country has a tundra climate, and in “Austral”, it is a cold semi-arid area with an extended surface of
 113 grassland, forest, and, to a lesser extent, savanna.

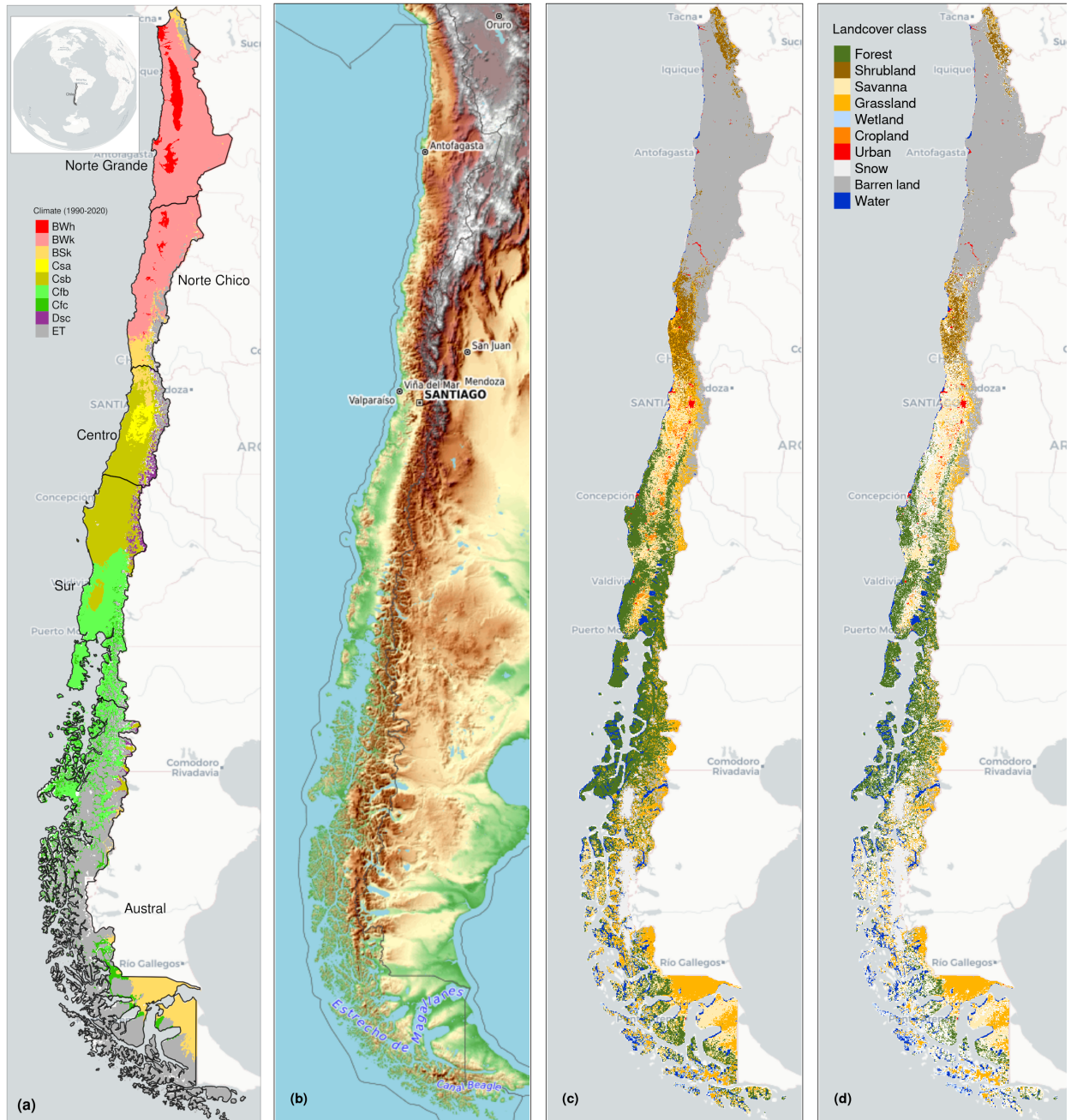


Figure 1: (a) Chile with the Koppen-Geiger climate classes and the five macrozones “Norte Grande”, “Norte Chico”, “Centro”, “Sur”, and “Austral”. (b) Topography reference map. (c) land cover classes for 2022. (d) Persistent land cover classes (> 80%) for 2001-2022

¹¹⁴ **3. Materials and Methods**

¹¹⁵ *3.1. Data*

¹¹⁶ *3.1.1. Gridded meteorological and vegetation data*

¹¹⁷ To analyze the LULCC, we use the IGBP scheme from the MCD12Q1 collection 6.1 from MODIS. This
¹¹⁸ product has a yearly frequency from 2001 to 2022. The IGBP defines 17 classes; from these, we regrouped
¹¹⁹ into ten macroclasses, as follows: classes 1-4 to forest, 5-7 to shrublands, 8-9 to savannas, 10 as grasslands,
¹²⁰ 11 as wetlands, 12 and 14 to croplands, 13 as urban, 15 as snow and ice, 16 as barren, and 17 to water
¹²¹ bodies. Thus, we have a land cover raster time series with the ten classes for 2001 and 2023. Prior to
¹²² using this class, we compared it with the types of land cover made by Zhao et al. (2016), which is a more
¹²³ detailed land cover map of Chile with a 30 m spatial resolution for 2012–2013. It reached a global accuracy
¹²⁴ of ~0.82. The procedure of validation is demonstrated in Section S1 of the supplementary material. To derive
¹²⁵ a proxy for vegetation productivity, we used the MOD13A3 collection 6.1 product from MODIS (Didan,
¹²⁶ 2015). It provides vegetation indices (NDVI and EVI) at 1km of spatial resolution and monthly frequency.
¹²⁷ The MOD13A3 and MCD12Q1 were retrieved from the online Data Pool, courtesy of the NASA EOSDIS
¹²⁸ Land Processes Distributed Active Archive Center (LP DAAC), USGS Earth Resources Observation and
¹²⁹ Science (EROS) Center, Sioux Falls, South Dakota, <https://lpdaac.usgs.gov/tools/data-pool/>.

Table 1: Description of the earth observation data used

Product	Sub-product	Variable	Spatial Resolution	Period	Units	Short Name
ERA5L		Precipitation	0.1°	1981-2023	mm	P
		Maximum temperature			°C	T _{max}
		Minimum temperature			°C	T _{min}
		Volumetric Soil Water Content at 1m			m3/m3	SM
ERA5L*	MOD13A3.061	Atmospheric Evaporative Demand	0.1°	1981-2023	mm	AED
MODIS		Normalized Difference Vegetation Index	1 km	2000-2023		NDVI
	MCD12Q1.061	land cover IGBP scheme		2001-2022		land cover

*Derived from ERA5L with Eq. 1.

¹³⁰ For soil moisture, water supply, and water demand variables, we used ERA5L (Muñoz-Sabater et al., 2021),
¹³¹ a reanalysis dataset that provides the evolution of the meteorological and soil moisture variables since 1950.
¹³² It has a spatial resolution of 0.1° (9 km), hourly frequency, and global coverage. We selected the variables
¹³³ for total precipitation, maximum and minimum temperature at 2 meters, and volumetric soil water layers
¹³⁴ between 0 and 100cm of depth (layer 1 to layer 3).

¹³⁵ *3.2. Land cover change and trend*

¹³⁶ To analyze the LULCC, we use the IGBP scheme from the MCD12Q1 collection 6.1 from MODIS. Zambrano
¹³⁷ et al. (2018) and Fuentes et al. (2021) have previously used this product for studies of drought and land
¹³⁸ cover. The MCD12Q1 has a yearly frequency from 2001 to 2022. The IGBP defines 17 classes; from these,
¹³⁹ we regrouped into ten macroclasses, as follows: classes 1-4 to forest, 5-7 to shrublands, 8-9 to savannas, 10
¹⁴⁰ as grasslands, 11 as wetlands, 12 and 14 to croplands, 13 as urban, 15 as snow and ice, 16 as barren, and 17
¹⁴¹ to water bodies. Thus, we have a land cover raster time series with the ten macroclasses for 2001 and 2023.
¹⁴² We validate the land cover macroclasses regarding a highly detailed (30 m of spatial resolution) land cover
¹⁴³ map made for Chile by Zhao et al. (2016) for 2013-2014. Our results showed a global accuracy of ~0.82 and
¹⁴⁴ a F1 score of ~0.66. Section S2 in the Supplementary Material shows the procedure for validation.

¹⁴⁵ Climate, vegetation development, seasonality, and changes in vegetation type all have an impact on the
¹⁴⁶ time series of NDVI. In this study, we want to examine the variation in vegetation productivity across various
¹⁴⁷ land cover types and how water demand, water supply, and soil moisture affect it. In order to avoid changes

148 due to a change in the land cover type that will wrongly impact NDVI, we developed a persistence mask for
 149 land cover for 2001–2022. Thereby, we reduce an important source of variation on a regional scale. Therefore,
 150 we generated a raster mask for IGBP MODIS per pixel using macroclasses that remained unchanged for at
 151 least 80% of the years (2001–2022). This enabled us to identify regions where the land cover macroclasses
 152 are persistent. We calculated the surface occupied per land cover class into the five macrozones (“Norte
 153 Grande” to “Austral”) per year for 2001–2023. After that, we calculated the trend’s change in surface per
 154 type. We used the Sen’ slope ([Sen, 1968](#)) based on Mann-Kendall ([Kendall, 1975](#)).

155 *3.3. Trend of drought and interaction to land cover change*

156 *3.3.1. Atmospheric Evaporative Demand (AED)*

157 In order to compute the drought indices that uses water demand, it is necessary to first calculate the AED.
 158 To do this, we employed the Hargreaves technique ([Hargreaves, 1994](#); [Hargreaves and Samani, 1985](#)), by
 159 applying the following equation:

$$AED = 0.0023 \cdot Ra \cdot (T + 17.8) \cdot (T_{max} - T_{min})^{0.5} \quad (1)$$

160 where Ra ($MJ\ m^2\ day^{-1}$) is extraterrestrial radiation; T , T_{max} , and T_{min} are mean, maximum, and
 161 minimum temperature ($^{\circ}C$). We calculate the centroid coordinates per pixel and use the latitude to estimate
 162 Ra .

163 We chose the method of Hargreaves to estimate AED because of its simplicity, which only requires tem-
 164 peratures and extrarrestrial radiation. Also, it has been recommended over other methods (e.g., Penman-
 165 Monteith) when the access to climatic variables is limited ([Vicente-Serrano et al., 2014](#)).

166 *3.3.2. Non-parametric calculation of drought indices*

167 To derive the drought indices of water supply and demand, soil moisture, and vegetation we used the ERA5L
 168 dataset and the MODIS product, with a monthly frequency for 1981–2023 and 2000–2023, respectively.

169 The drought indices correspond to a historical anomaly with regard to a variable (e.g., meteorological,
 170 vegetation, or soil moisture). To account for the anomaly, the common practice is to derive it following
 171 a statistical parametric methodology in which it is assumed that the statistical distribution of the data is
 172 known ([Heim \(2002\)](#)). A wrong decision is usually the highest source of uncertainty ([Laimighofer and Laaha
 173 \(2022\)](#)). In the case of Chile, due to its high degree of climatic variability, it is complex to choose a proper
 174 distribution without previous research. Here, we follow a non-parametric methodology for the calculation
 175 of the drought indices, in a similar manner as the framework proposed by [Farahmand and AghaKouchak
 176 \(2015\)](#); [Hobbins et al. \(2016\)](#); [McEvoy et al. \(2016\)](#).

177 For the purpose of monitoring water supply drought, we used the well-known Standardized Precipitation
 178 Index (SPI), which the World Meteorological Organization (WMO) recommended. The SPI solely relies on
 179 precipitation data. Also, it has been used worldwide for the study of drought, including in Chile ([Garreaud
 180 et al. \(2017\)](#); [Zambrano et al. \(2017\)](#)). The primary cause of drought is precipitation anomalies, and
 181 temperature usually makes it worse ([Luo et al. 2017](#)). Nowadays, there is an increase in attention toward
 182 using water demand separately to monitor droughts. ([Vicente-Serrano et al. \(2020\)](#); [Noguera et al. \(2022\)](#)).
 183 Thus, to evaluate water demand, we chose the Evaporative Demand Drought Index (EDDI), developed
 184 by [Hobbins et al. \(016\)](#) and [McEvoy et al. \(2016\)](#), which is based on the AED. EDDI is currently used for
 185 monitoring drought in the United States (<https://psl.noaa.gov/eddi/>). In our case, we used only temperature
 186 for AED, a difference from the original formulation of EDDI, which also considered wind besides temperature.
 187 To consider the combined effect of water supply and demand, we selected the SPEI, which corresponds to
 188 a balance between precipitation and AED. [Vicente-Serrano et al. \(2010\)](#) proposed the SPEI, and it has
 189 improved the SPI by incorporating temperature for drought monitoring. For SPEI, an auxiliary variable D
 190 = P -AED is calculated. Soil moisture is the main driver of vegetation productivity, particularly in semi-arid
 191 regions ([Li et al. \(2022\)](#)). Hence, for soil water drought, we used the SSI (Standardized Soil Moisture Index)

¹⁹² (Hao and AghaKouchak 2013; A. AghaKouchak 2014) which is a multi-scale index similar to SPI, SPEI, and
¹⁹³ EDDI. In our case, for the SSI, we used the average soil moisture from ERA5L at 1m depth. Finally, for
¹⁹⁴ the proxy of productivity, we used the zcNDVI proposed by Zambrano et al. (2018) which will be derived
¹⁹⁵ from the NDVI retrieved from MOD13A1.

¹⁹⁶ To derive the drought indices, first we must calculate the sum of the variables with regard to the time scale
¹⁹⁷ (s). In this case, for generalization purposes, we will use V , referring to variables P , AED , D , $NDVI$, and
¹⁹⁸ SM (Table 1). We cumulated each V over the time series of n values (months), and for the time scales s :

$$A_{si} = \sum_{i=n-s-i+2}^{n-i+1} V_i \quad \forall i \geq n - s + 1 \quad (2)$$

¹⁹⁹ The A_{si} corresponds to a moving window (convolution) that sums the variable for time scales s from the
²⁰⁰ last month, month by month, until the first month in which it could sum for s months. Once the variable
²⁰¹ is cumulated over time for the scale s . Thus, the empirically derived probabilities are obtained through an
²⁰² inverse normal approximation (Abramowitz and Stegun, 1968). Then, we used the empirical Tukey plotting
²⁰³ position (Wilks, 2011) over A_i to derive the $P(A_i)$ probabilities across a period of interest:

$$P(A_i) = \frac{i - 0.33}{n + 0.33} \quad (3)$$

²⁰⁴ The drought indices SPI , $SPEI$, $EDDI$, SSI , and $zcNDVI$ are obtained following the inverse normal
²⁰⁵ approximation:

$$DI(A_i) = W - \frac{C_0 + C_1 \cdot W + c_2 \cdot W^2}{1 + d_1 \cdot W + d_2 \cdot W^2 + d_3 \cdot W^3} \quad (4)$$

²⁰⁶ DI is referring to the drought index calculated for the variable V . The values for the constants are:
²⁰⁷ $C_0 = 2.515517$, $C_1 = 0.802853$, $C_2 = 0.010328$, $d_1 = 1.432788$, $d_2 = 0.189269$, and $d_3 = 0.001308$. For
²⁰⁸ $P(A) \leq 0.5$, $W = \sqrt{-2 \cdot \ln(P(A_i))}$, and for $P(A_i) > 0.5$, replace $P(A_i)$ with $1 - P(A_i)$ and reverse the sign
²⁰⁹ of $DI(A_i)$.

²¹⁰ The drought indices were calculated for time scales of 1, 3, 6, 12, 24, and 36 months at a monthly frequency
²¹¹ for 1981–2023 in order to be used for short- to long-term evaluation of drought. In the case of the proxy of
²¹² vegetation productivity (zcNDVI) it was calculated for a time scale of six months at monthly frequency for
²¹³ 2000–2023. For zcNDVI, we test time scales of 1, 3, 6, and 12 months; we choose to use six months because
²¹⁴ that shows a more robust representation of vegetation productivity due to the seasonality of vegetation in
²¹⁵ Chile.

²¹⁶ 3.3.3. Trend of drought indices

²¹⁷ To estimate if there are significant positive or negative trends for the drought indices, we used the non-
²¹⁸ parametric test of Mann-Kendall (Kendall, 1975). To determine the magnitude of the trend, we used Sen's
²¹⁹ slope (Sen, 1968). Some of the advantages of applying this methodology are that the Sen's slope is not
²²⁰ affected by outliers as regular regression does, and it is a non-parametric method that is not influenced by
²²¹ the distribution of the data. We applied Mann-Kendall to see if the trend was significant and Sen's slope
²²² to estimate the magnitude of the trend. We did this to the six time scales from 1981 to 2023 (monthly
²²³ frequency) and the indices SPI, EDDI, SPEI, and SSI. Thus, we have trends per index and time scale (24 in
²²⁴ total). Then, we extracted the trend aggregated by macrozone and per land cover persistent macroclasses.

225 3.3.4. *Intercation drought indices and land cover change*

226 We wanted to explore the relationship between the trend in land cover classes and the trend in the drought
227 indices. For this purpose, in order to have more representative results, we conducted the analysis over sub-
228 basins within continental Chile. We use 469 basins, which have a surface area between 0.0746 and 24,000
229 (km^2), and a median area of 1,249 (km^2). For each basin, we calculate the relative trend per land cover
230 type, considering the proportion of the type relative to the total surface of the basin. Then, we extracted
231 per basin the average trend of the drought indices SPI, SPEI, EDDI, SSI, and all their time scales 1, 3, 6,
232 12, 24, and 36. Also, we extracted the average trend in the proxy of vegetation productivity (zcNDVI). We
233 wanted to analyze which drought indices and time scales have a major impact on changes in land cover type.

234 We have 25 predictors, which are drought indices and vegetation productivity. We analyzed the 25 predictors
235 per type of landcover. For the analysis, we selected the method of random forest ([Ho \(1995\)](#)). Because
236 it allows to find no linear relationship, it reduces overfitting and can derive the feature importance, which
237 helps for a better understanding of the relationships. The importance of the variable is calculated by per-
238 muting out-of-bag (OOB) data per tree and calculating the mean standard error in the OOB. Then the
239 same is done after permuting each predictor variable. Random forest uses multiple decision trees and allows
240 for classification and regression.

241 We analyzed the 25 predictors per type of landcover, thus running six models. We used random forests for
242 regression and trained 1000 forests. For more reliable results for the important variables, we resampled by
243 creating ten folds, running a random forest per fold, and calculating the r-squared (rsq), root mean square
244 error (RMSE), and variable importance ten times.

245 3.4. *Drought impacts on vegetation productivity within land cover*

246 We analyzed the trend of vegetation productivity over the unchanged land cover macroclasses. This way,
247 we tried to reduce the noise in the vegetation due to a change in land cover from year to year. To achieve
248 this, we will use the persistent mask of land cover macroclasses, which are the types that remain more than
249 80% of the time for 2001–2022. We used this to evaluate the trend in zcNDVI per land cover class and
250 macrozone.

251 We examine the drought indices of water demand, water supply, soil moisture, and their connection with
252 vegetation productivity to investigate two main questions: i) whether short-term or long-term time scales
253 have a greater impact on vegetation across Chile and its specific regions; and ii) the spatial variation
254 in the strength of the correlation between the variables and time scales. Then, we will summarize for
255 each land cover class and macrozone. Thus, we will be able to advance in understanding how climate
256 is affecting vegetation, considering the impact on the five macroclasses of vegetation: forest, cropland,
257 grassland, savanna, and shrubland.

258 We conducted an analysis on the linear correlation between the indices SPI, SPEI, EDDI, and SSI over
259 time periods of 1, 3, 6, 12, 24, and 36 months, and zcNDVI. The objective is to determine the impact of
260 soil moisture and water demand and supply on vegetation productivity. We used a method similar to that
261 used by [Meroni et al. \(2017\)](#) which compared the SPI with the cumulative FAPAR (Fraction of Absorbed
262 Photosynthetically Active Radiation). A pixel-to-pixel linear correlation analysis was performed for each
263 index within the persistent mask of land cover macroclasses. To begin, the Pearson coefficient of correlation
264 is computed for each of the six time scales. A significant time scale is identified as the one that attains the
265 highest correlation ($p < 0.05$). Subsequently, the Pearson correlation coefficient corresponding to the time
266 scales at which the value peaked was extracted. As a result, for each index, we generated two raster maps:
267 1) containing the raster with values of the time scales that reached the maximum correlation, and 2) having
268 the value of the correlation obtained.

269 3.5. *Software and packages used*

270 For the downloading, processing, and analysis of the spatio-temporal data, we used the open source software
271 for statistical computing and graphics, R ([R Core Team, 2023](#)). For downloading ERA5L, we used the

272 {ecmwfr} package (Hufkens et al., 2019). For processing raster data, we used {terra} (Hijmans, 2023) and
 273 {stars} (Pebesma and Bivand, 2023). For managing vectorial data, we used {sf} (Pebesma, 2018). For
 274 the calculation of AED, we used {SPEI} (Beguería and Vicente-Serrano, 2023). For mapping, we use {tmap}
 275 (Tennekes, 2018). For data analysis, the suite {tidyverse} (Wickham et al., 2019) was used.

276 4. Results

277 5. Land cover change and trend

Table 2: Surface of the land cover class that persist during 2001-2022

macrozone	Surface [km ²]					
	Forest	Cropland	Grassland	Savanna	Shrubland	Barren land
Norte Grande			886		7,910	171,720
Norte Chico		90	4,283	589	16,321	84,274
Centro	3,739	1,904	7,584	19,705	844	12,484
Sur	72,995	1,151	7,198	15,906		2,175
Austral	60,351		54,297	19,007	249	7,218
Total	—	137,085	3,145	74,247	55,206	25,324
						277,870

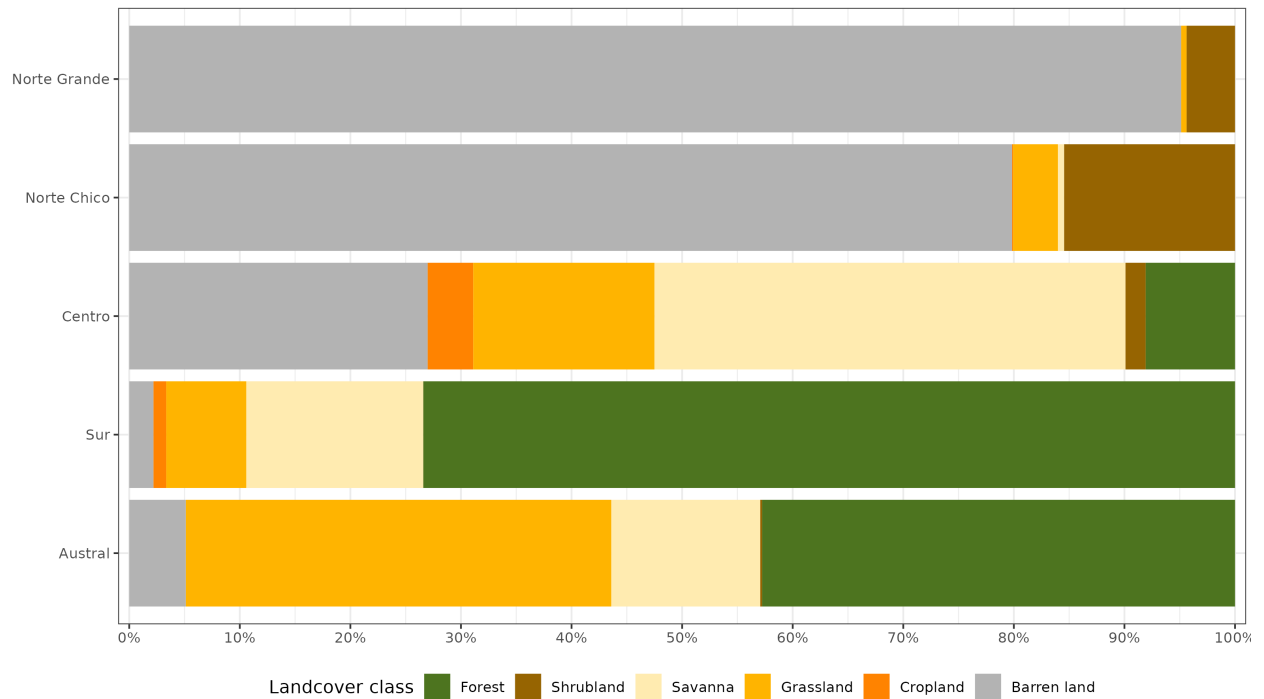
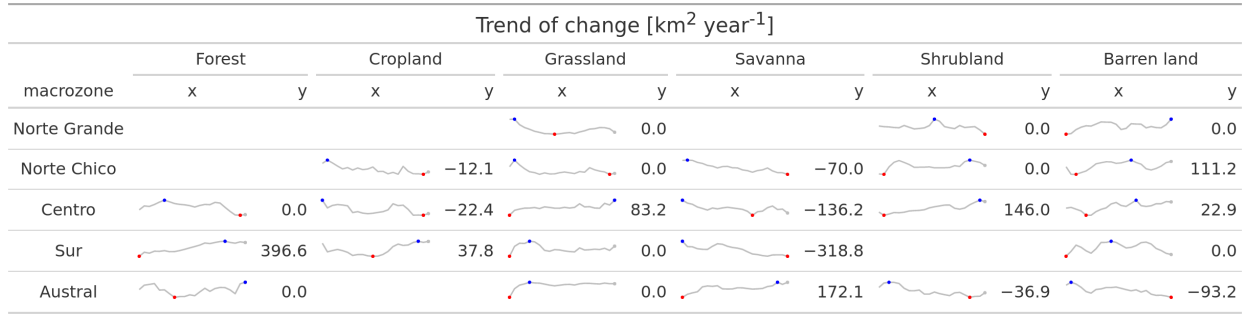


Figure 2: Proportion of land cover class from the persistent land cover for 2001-2022 (>80%) per macrozone

278 For vegetation, we obtained and use hereafter five macroclasses of land cover from IGBP MODIS: forest,
 279 shrubland, savanna, grassland, and croplands. Figure 1c shows the spatial distribution of the macroclasses
 280 through Chile for the year 2022. Figure 1d shows the macroclasses of land cover persistance (80%) during
 281 2021–2022, respectively (Table 2). Within continental Chile, barren land is the land cover class with the
 282 highest surface area (277,870 km²). The largest type of vegetation, with 137,085 km², is forest. Grassland
 283 (74,247 km²), savanna (55,206 km²), shrubland (25,341 km²), and cropland (3,146 km²) are the other types

(Table 2). The macrozones with major changes for 2001–2022 were “Centro,” “Sur,” and “Austral,” with 36%, 31%, and 34% of their surface changing the type of land cover, respectively (Figure 1 and Table 3). Figure 2 shows the summary of the proportion of surface per land cover class and macrozone, derived from the persistence mask over continental Chile.

Table 3: The value of Sen’s slope trend next to the time-series plot of surface per land cover class (IGBP MCD12Q1.016) for 2001–2022 through Central Chile. Values of zero indicate that there was not a significant trend. Red dots on the plots indicate the maximum and minimum values of surface.



The “Norte Chico” shows an increase in barren land of $111 \text{ km}^2 \text{ yr}^{-1}$ and a reduction in the class savanna of $70 \text{ km}^2 \text{ yr}^{-1}$. In the “Centro” and “Sur,” there are changes with an important reduction in savanna ($136 \text{ to } 318 \text{ km}^2 \text{ yr}^{-1}$), and an increase in shrubland and grassland. Showing a change for more dense vegetation types. It appears to be a shift in the area cultivated (croplands) from the “Centro” to the “Sur.” Also, there is a high increase in forest ($397 \text{ km}^2 \text{ yr}^{-1}$) in the “Sur,” replacing the savanna lost (Table 3).

5.1. Trend of drought and interaction to land cover change

5.1.1. Trend of drought indices

Figure 3 shows the spatial variation of the trend for the drought indices from short- to long-term scales. SPI and SPEI have a decreasing trend from “Norte Chico” to “Sur.” However, there is an increasing trend in “Austral.” The degree of the trend is stronger at higher time scales. The SSI indicates that in “Norte Grande,” there are surfaces that have increased in the southwest part and in the northeast have decreased, and is shown for all time scales. Similar to SPI and SPEI, SSI decreases at higher time scales. EDDI showed a positive trend for the whole of continental Chile, with a higher trend toward the north and a descending gradient toward the south. The degree of trend increases at higher time scales.

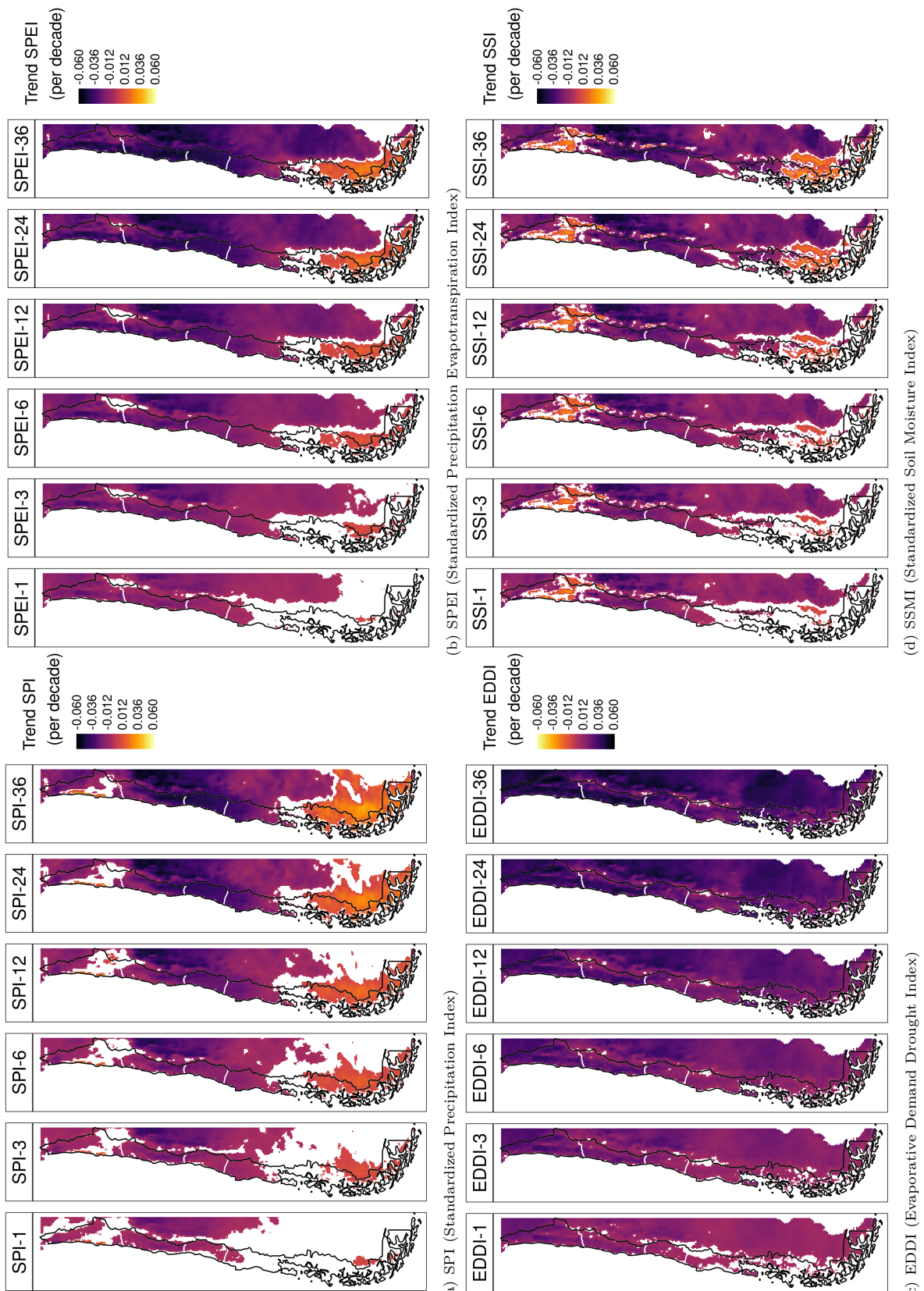


Figure 3: Linear trend of the drought index (*) at time scales of 1, 3, 6, 12, 24, and 36 months for 1981-2023

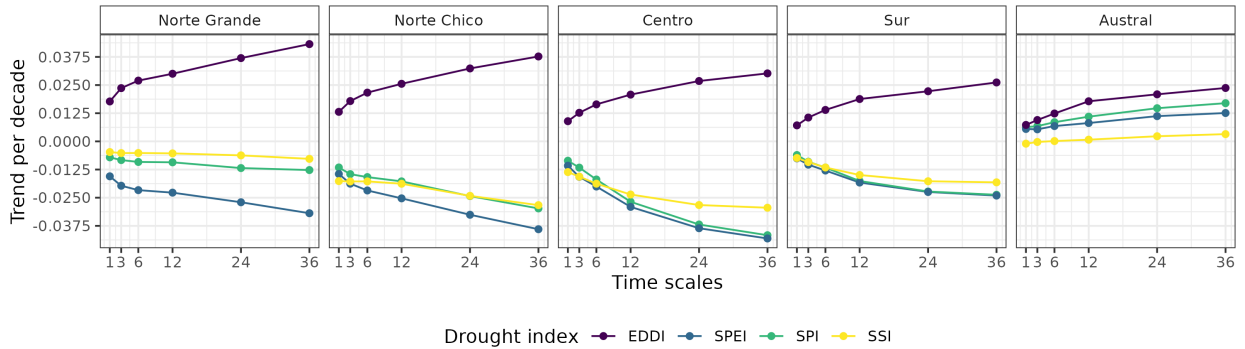


Figure 4: Trend per decade for the drought indices SPI, EDDI, SPEI, and SSI aggregated by macrozone.

In Figure 4, the averaged aggregation per macrozone, drought index, and time scale are shown. The macrozones that have the lowest trend are “Norte Chico” and “Centro,” where the SPI, SPEI, and SSI show that it decreases at longer time scales. Potentially explained due to the prolonged reduction in precipitation that has affected the hydrological system in Chile. At 36 months, it reaches trends between -0.03 and -0.04 (z-score) per decade for SPI, SPEI, and SSI. For “Sur,” the behavior is similar, decreasing at longer scales and having between -0.016 and -0.025 per decade for SPI, SPEI, and SSI. “Norte Grande” has the highest trend at 36 months for EDDI (0.042 per decade), and “Centro” has the lowest for SPI and SPEI. In “Norte Grande” and “Norte Chico,” which are in a semi-arid climate, it is evident that the EDDI has an effect on the difference between the SPI and SPEI index, which is not seen in the other macrozones. Contrary to the other macrozones, “Austral” showed an increase in all indices, being the highest for EDDI at 36 months (0.025) and the lowest for SSI, which shows only a minor increase in the trend.

5.1.2. Relationship between drought indices and land cover change

According to Table 4, barren land is the type of land cover that is most affected by the trend of drought indices that reach a $rsq = 0.4$. This is attributed to the fact that it is linked to short-term deficits in precipitation (SPI-6 and SPEI-6) and long-term AED (EDDI-12 and EDDI-24). The trend in drought indices accounts for about a quarter of the change in grassland, savanna, and shrubland types. These types are most affected by the increase in short-term water demand (EDDI-6). The changes in forests are strongly impacted by the increase in long-term water demand (EDDI-36). The trend in croplands cannot be attributed to variations in water demand, water supply, soil moisture, or vegetation productivity.

Table 4: The five most important trends of drought indices in estimating the landcover trend per land cover type and the r-squared (rsq) reached by each random forest model.

Position	Forest ($rsq=0.25$)	Cropland ($rsq=0.06$)	Grassland ($rsq=0.27$)	Savanna ($rsq=0.22$)	Shrubland ($rsq=0.29$)	Barren_land ($rsq=0.4$)
1	EDDI-36	EDDI-36	EDDI-6	EDDI-6	EDDI-6	SPI-6
2	EDDI-24	SSI-36	EDDI-12	EDDI-12	SPI-36	SPEI-6
3	EDDI-12	EDDI-24	EDDI-24	EDDI-24	SPEI-36	EDDI-24
4	SSI-36	SSI-24	EDDI-3	EDDI-3	EDDI-3	EDDI-12
5	SSI-12	SPEI-36	EDDI-36	EDDI-36	SPI-24	SPI-36

We look at the relationship between drought index and land cover change in Figure 5 by comparing the trends in land cover change (in terms of the total surface area per land cover type and macrozone) and drought indexes. Figure 5 shows that the negative trends in cropland (-0.029) and savanna (-0.026) in

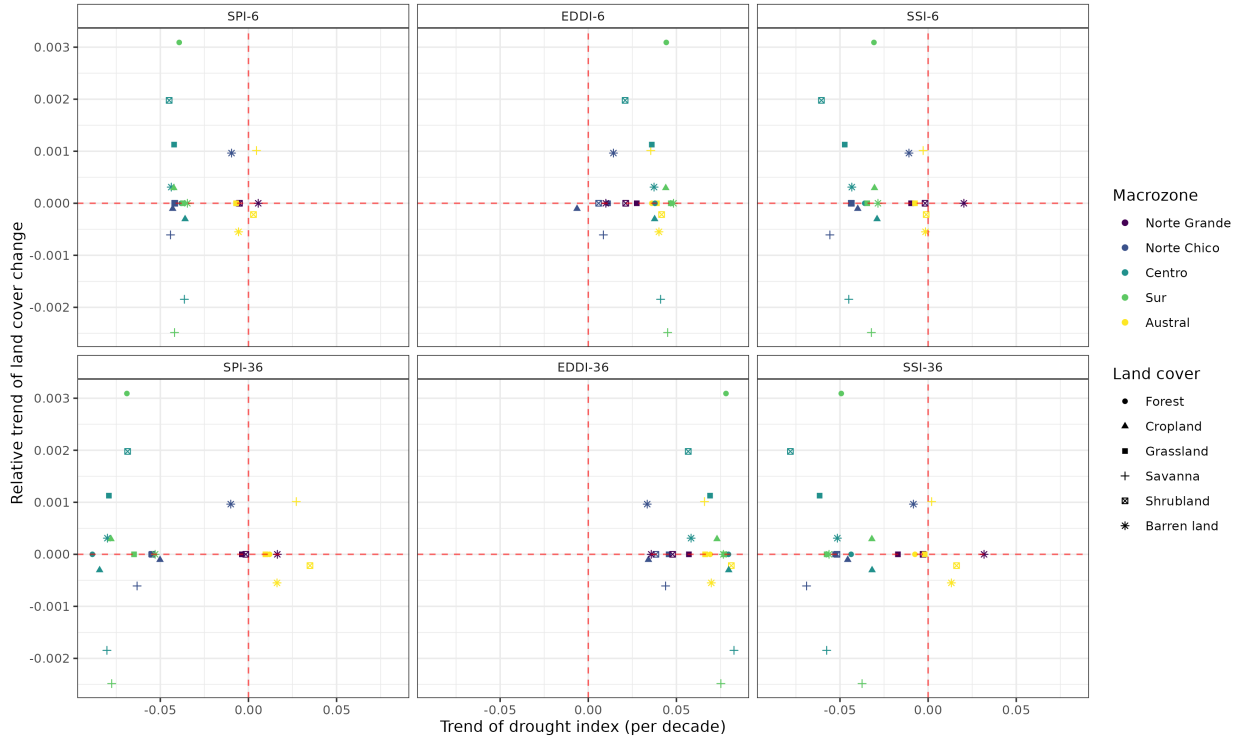


Figure 5: Relationship between the trend in land cover change and the trend in drought indices for the five macrozones. Vertical panels correspond to 1, 3, 6, 12, 24, and 36 months of the time scale by drought index. Horizontal panels show each drought index

“Norte Chico” are the highest and are associated with an increase trend in EDDI and a decreasing trend in SPI, SPEI, and SSI. On the contrary, the shrubland in “Centro” has an increase (0.04) linked to a decrease in SPI, SPEI, and SSI and to an increase in EDDI. In “Austral,” the positive trend in shrubland fits with the positive trend in all the drought indices. The rest of the land cover types in the macrozones show weak associations with water supply, water demand, or soil moisture drought indices.

5.2. Drought impacts on vegetation productivity within land cover

5.2.1. Vegetation productivity

In Figure 6 it is showed the spatial map of trends in zcNDVI ([fig-zcNDVI_var]a) and the temporal variation of zcNDVI within the aggregated macrozones ([fig-zcNDVI_var]b). In “Norte Grande,” vegetation productivity, as per the z-index, exhibits a yearly increase of 0.02 with respect to grassland and shrubland categories. There is a negative trend in “Norte Chico” with -0.04 and “Centro” with -0.02 per decade. In “Norte Chico,” savanna (-0.05) has the lowest trend, and the rest of the types are around -0.04. In “Centro,” shrubland reaches -0.06, grassland -0.05, and croplands and savanna -0.01 per decade. This could be associated either with a reduction in vegetation surface, a decrease in biomass, or browning (Miranda et al., 2023). Vegetation reached its lowest values since the year 2019, with an extreme condition in early 2020 and 2022 in the “Norte Chico” and “Centro”. The “Sur” and “Austral” show a positive trend of around 0.016 per decade (Figure 6). Despite the croplands suffering from drought just as badly as the native vegetation in “Norte Chico,” the savanna and shrubland appears to be the region most affected by a negative trend in vegetation productivity.

5.2.2. Correlation between vegetation productivity and drought indices

Figure 7 is a map that shows the highest coefficient of determination (r^2 , or rsq) found in the regression analysis between different drought indicators and plant productivity over time. The spatial

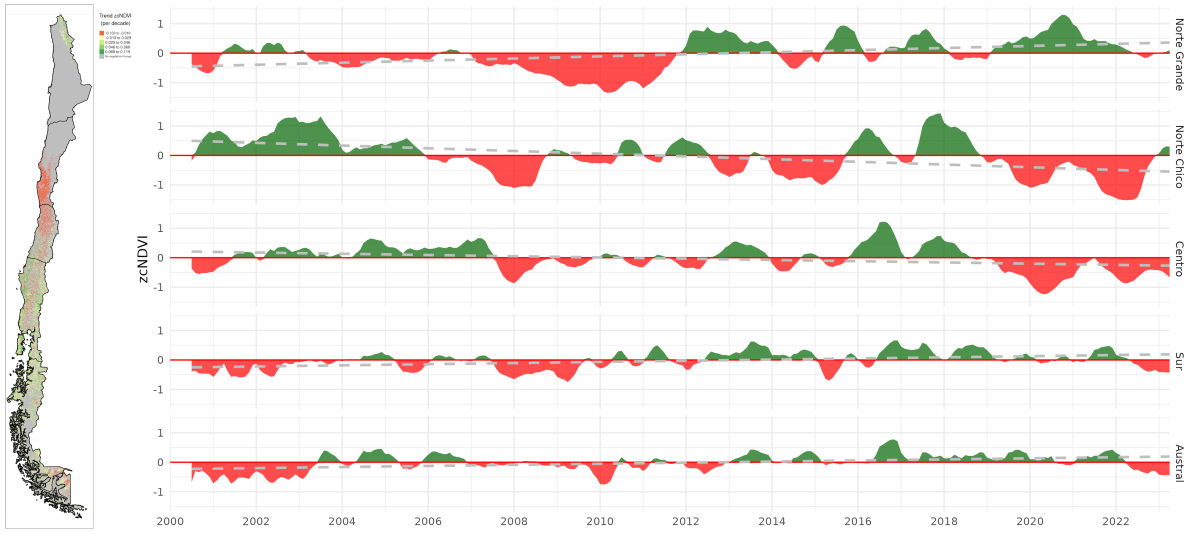


Figure 6: (a) Map of the linear trend of the index zcNDVI-6 for 2001–2023. Greener colors indicate a positive trend; redder colors correspond to a negative trend and a decrease in vegetation productivity. Grey colors indicate either no vegetation or a change in land cover type for 2001–2022. (b) Temporal variation of zcNDVI-6 aggregated at macrozone level within continental Chile. Each horizontal panel corresponds to a macrozone from ‘Norte Grande’ to ‘Austral’.

346 variation of time scales reached per index is mostly for time scales above 12 months. In the case of SSI,
 347 the predominant scales are 6 and 12 months. For all indices, to the north, the time scales are higher and
 348 diminish toward the south until the south part of “Austral” increases. In Figure 8, the map of Pearson
 349 correlation values is shown. The EDDI reached correlations above 0.5 between “Norte Chico” and “Sur.”
 350 The correlation changes from negative to positive toward the Andes Mountains and to the sea, just as in
 351 the northern part of “Austral.” The SPI and SPEI have similar results, with the higher values in “Norte
 352 Chico” and “Centro” being higher than 0.6. Following a similar spatial pattern as EDDI. The SSI showed
 353 to be the index that has a major spatial extension with a higher correlation. It has a similar correlation to
 354 SPI and SPEI for “Norte Chico” and “Sur,” but has improvements for “Sur.”

Table 5: Summary per land cover macroclass and macrozone regarding the correlation between zcNDVI with the drought indices EDDI, SPI, SPEI, and SSI for time scales of 1, 3, 6, 12, 24, and 36. The numbers in each cell indicate the time scale that reached the maximum correlation for the land cover and macrozone, and the color indicates the strength of the r-squared obtained with the index and the time scale.

	Forest				Cropland				Grassland				Savanna				Shrubland			
macrozone	EDDI	SPI	SPEI	SSI	EDDI	SPI	SPEI	SSI	EDDI	SPI	SPEI	SSI	EDDI	SPI	SPEI	SSI	EDDI	SPI	SPEI	SSI
Norte Grande									36	36	36	12					36	12	36	12
Norte Chico					36	36	12	12	36	36	24	12	36	24	24	12	36	36	24	12
Centro	36	36	12	6	12	12	6	6	12	12	12	36	12	12	12	36	24	24	12	
Sur	36				6	6	6	6	6	6	6	12	6	6	6	6				
Austral	6	6									6	12	12	6	6	12	12	6	6	6
r-squared																				

355 In Table 5, we aggregate per macrozone and landcover the correlation analysis presented in Figure 7 and

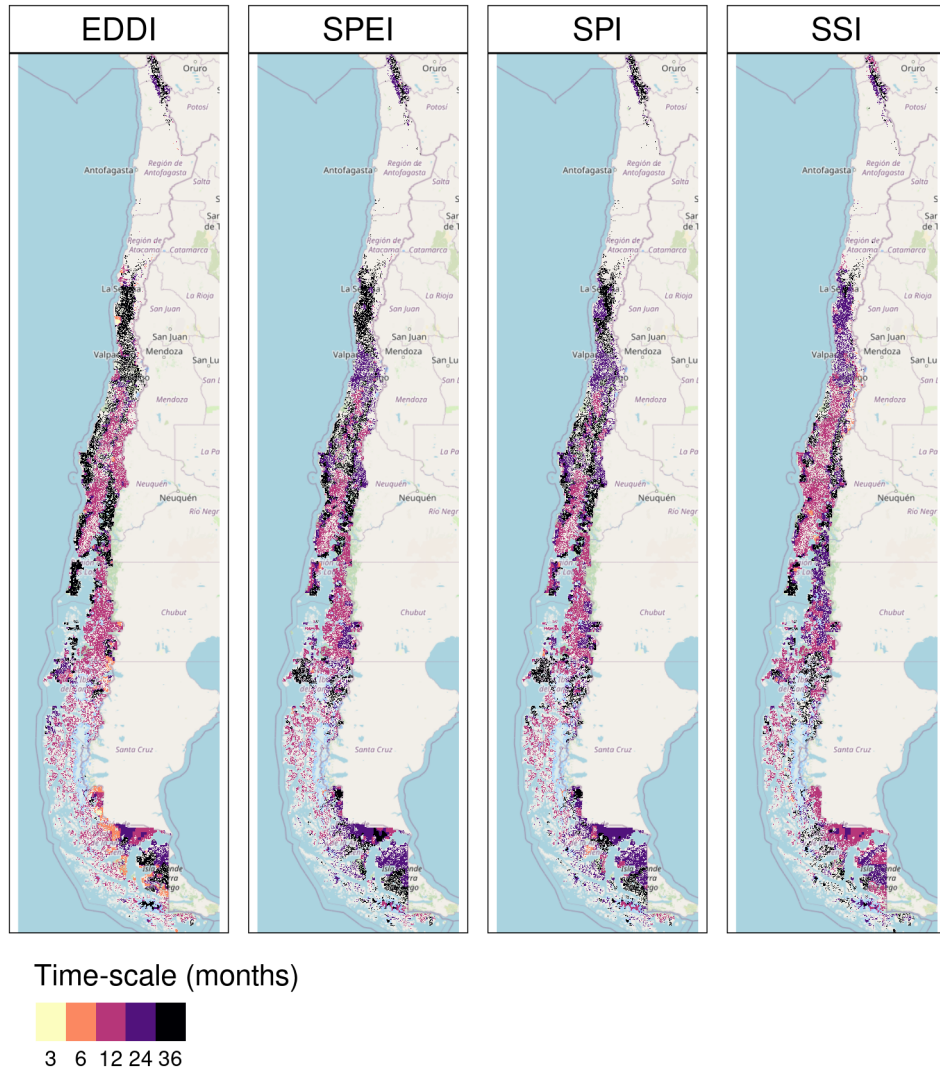


Figure 7: Time scales per drought index that reach the maximum coefficient of determination

356 Figure 8. According to what is shown, forests seem to be the most resistant to drought. Showing that
 357 only “Centro” is slightly ($rsq = 0.25$) impacted by a 12-month soil moisture deficit (SSI-12). In the “Norte
 358 Chico” and to a lesser extent in the “Norte Grande,” it is evident that a SSI-12 with a $rsq = 0.45$ and a
 359 decrease in water supply (SPI-36 and SPEI-24 with $rsq = 0.28$ and 0.34 , respectively) have an impact on
 360 grasslands. However, this type was unaffected by soil moisture, water supply, or demand in macrozones
 361 further south. The types that show to be most affected by variation in climate conditions are shrublands,
 362 savannas, and croplands. For savannas in “Norte Chico,” the SSI-12 and SPI-24 reached an rsq of 0.74
 363 and 0.58 , respectively. This value decreases to the south, but the SSI-12 is still the variable explaining
 364 more of the variation in vegetation productivity ($rsq = 0.45$ in “Centro” and 0.2 in “Sur”). In the case
 365 of croplands, the SPEI-12, SPI-36, and SSI-12 explain between 45% and 66% of the variability in “Norte
 366 Chico.” The type of land most impacted by climatic variation was shrubland, where soil moisture explained
 367 59% and precipitation, 37% , in “Norte Chico” and “Centro,” with SSI-12 being the most relevant variable,
 368 then SPI-36 in “Norte Chico” and SPI-24 in “Sur.”

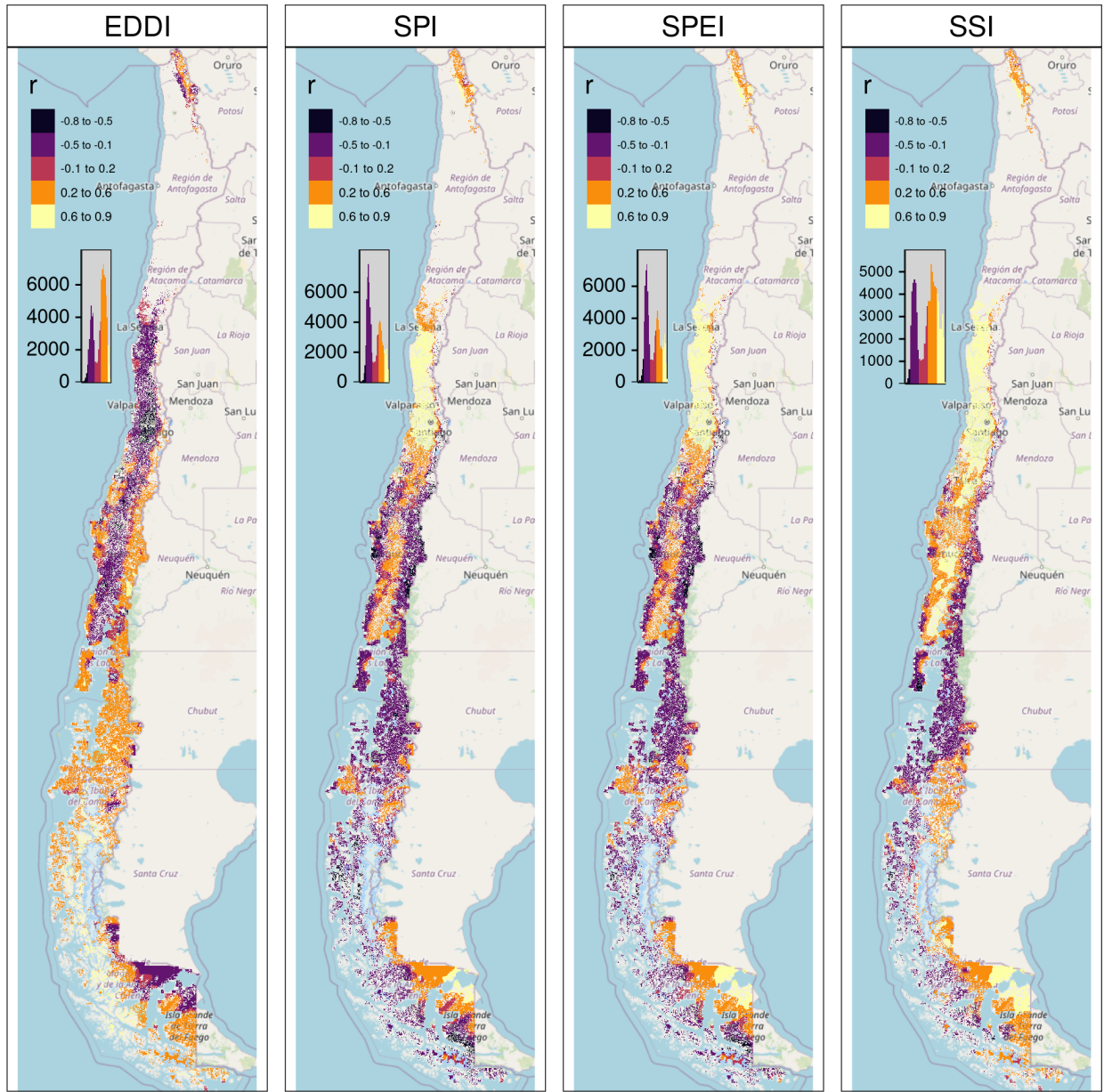


Figure 8: Pearson correlation value for the time scales and drought index that reach the maximum coefficient of determination

369 6. Discussion

370 6.1. Drought trend and attribution to land cover

371 Vicente-Serrano et al. (2022), in a study at the global scale of drought trends, indicate that there have not
 372 been significant trends in meteorological drought since 1950. Also, state that the increase in hydrological
 373 trend in some parts of the globe (northeast Brazil and the Mediterranean region) is related to changes in land
 374 cover and specifically to the rapidly increasing irrigated area, which consequently increases water extraction.
 375 Kogan et al. (2020) analyzed the agricultural drought impact globally and in the main grain producer
 376 countries, finding that “since 1980, the Earth warming has not changed the drought area or intensity.” In
 377 our study, we considered the variation in vegetation productivity in Chile for areas without changes in land

378 cover, to avoid misleading conclusions that could be related to the increase in water demand due to land
379 cover change. Our results show a contrasting perspective. There has been a significant trend in the decline
380 of vegetation productivity (zcNDVI) since 2000 for “Norte Chico” and “Centro,” which has been extreme
381 between 2020 and 2022, seemingly due to an intense hydrological drought due to the persistence of the mega
382 drought ([Garreaud et al., 2017](#)). However, a rise in irrigated land doesn’t seem to have an impact on this
383 hydrological drought. Despite using the persistence mask for vegetation’s trend analysis, cropland, which
384 is the most water-demand type, showed a decrease trend in “Norte Chico” and “Centro.” Also, there was
385 an increase in barren land for both types. These changes are associated with a decrease in water demand
386 from vegetation. Nonetheless, we used the persistent land cover to ensure that the pixel has the same class;
387 in the case of croplands, it could happen that some areas had changed crops for others with higher water
388 consumption and consequently increase water demand. But this effect should be minor compared to the
389 results from land cover change at this scale of analysis.

390 On the other hand, for “Norte Chico” and “Centro,” our results show a decrease in trends of water supply
391 (SPI and SSI), which are higher at larger time scales, which is evidence of the hydrological drought. We say
392 that what happened in central Chile goes against what has been found on a global scale ([Vicente-Serrano et al., 2022](#); [Kogan et al., 2020](#)). This shows that the main cause of the hydrological drought in Chile was
393 a steady drop in water supply made worse by an increase in AED, but it seems that in zones most affected
394 by drought, the main cause is not an increase in water demand by vegetation like irrigated crops. Finally,
395 north-central Chile has experienced a decline in vegetation productivity across all macroclasses, which is
396 primarily attributable to variations in water supply and soil moisture. An increase in water demand, such
397 as an increase in the surface area of irrigated crops, could strengthen this trend.

399 *6.2. Land cover types and their impact by drought*

400 We discovered that croplands, savannas, and shrubland are the most susceptible to climatic changes and are
401 most affected by the 12-month soil moisture deficit. In a study in the Yangtze River Basin in China, [Jiang et al. \(2020\)](#) analyzed the impact of drought on vegetation using the SPEI and the Enhanced Vegetation
402 Index (EVI). They found that cropland was more sensitive to drought than grassland, showing that cropland
403 responds strongly to short- and medium-term drought (< SPEI-6). In our case, the SPEI-12 was the one that
404 most impacted the croplands in “Norte Chico” and “Centro.” In general, most studies show that croplands
405 are most sensitive to short-term drought (< SPI-6) ([Zambrano et al., 2016](#); [Potopová et al., 2015](#); [Dai et al., 2020](#); [Rhee et al., 2010](#)). Short-term precipitation deficits impact soil water, and thus less water is available
406 for plant growth. However, we found that in “Norte Chico,” an SPI-36 and SPEI-12 had a higher impact,
407 which are associated with hydrological drought (long-term), and in “Centro,” an SPI-12 and SPEI-12. Thus,
408 we attribute this impact to the hydrological drought that has decreased groundwater storage ([Taucare et al., 2024](#)), which in turn is impacted by long-term deficits, and consequently, the vegetation is more dependent on
409 groundwater. In “Sur” and “Austral,” the correlations between drought indices and vegetation productivity
410 decrease, as do the time scales that reach the maximum r-squared. What can be explained is that, south of
411 “Centro,” predominate forest and grassland, the most resistant types. Also, drought episodes have been less
412 frequent and intense. The drought episodes have had a lower impact on water availability for vegetation.

416 According to [Senf et al. \(2020\)](#), severe drought conditions in Europe are a significant cause of tree mortality.
417 However, we found that forest is the type of land cover macroclass less affected by variation in drought indices,
418 being the most resistant land cover class to drought. Supporting this is [Fathi-Taperasht et al. \(2022\)](#), who
419 assert that Indian forests are the most drought-resistant and recover rapidly. Similarly, the work of [Wu et al. \(2024\)](#), who analyzed vegetation loss and recovery in response to meteorological drought in the humid
420 subtropical Pearl River basin in China, indicates that forests showed higher drought resistance. Using
421 Vegetation Optical Depth (VOD), kNDVI, and EVI, [Xiao et al. \(2023\)](#) test the resistance of ecosystems
422 and find that ecosystems with more forests are better able to handle severe droughts than croplands. They
423 attribute the difference to a deeper rooting depth of trees, a higher water storage capacity, and different
424 water use strategies between forest and cropland ([Xiao et al., 2023](#)).

426 In contrast to what we obtained, [Venegas-González et al. \(2023\)](#), who studied *Cryptocarya alba* and

427 Beilschmiedia miersii (both from the Lauraceae family) that live in sclerophyllous forests in Chile, found
428 that the trees' overall growth had slowed down. This could mean that the natural dynamics of their forests
429 have changed. They attributed it to the cumulative effects of the unprecedented drought (i.e., hydrological
430 drought). Thus, we attribute that forest to being the most resistant to drought, due to the fact that most
431 of the species comprising it are highly resilient to water scarcity compared to the other land cover classes.
432 Nonetheless, if we want to go deep in our analysis, we should use earth observation data that is able to
433 capture a higher level of detail. For example, when we used MOD13A3 with a 1km spatial resolution to
434 measure vegetation condition, it took the average condition of 1 square kilometer. Then, to use remote
435 sensing to look at how a certain type of forest (like sclerophyllous forest) changes in response to drought on
436 a local level, we should use operational products with higher spatial resolutions, like those from Landsat or
437 Sentinel. This will let us do a more thorough analysis.

438 *6.3. Soil moisture, vegetation productivity, and agricultural drought.*

439 The main external factors that affect biomass production by vegetation are actual evapotranspiration and
440 soil moisture, and the rate of ET in turn depends on the availability of water storage in the root zone.
441 Thus, soil moisture plays a key role in land carbon uptake and, consequently, in the production of biomass
442 ([Humphrey et al., 2021](#)). Moreover, [Zhang et al. \(2022\)](#) indicate there is a bidirectional causality between
443 soil moisture and vegetation productivity. Lastly, some studies have redefined agricultural drought as soil
444 moisture drought from a hydrological perspective ([Van Loon et al., 2016](#); [Samaniego et al., 2018](#)). Even
445 though soil moisture is the external factor most determinant of vegetation biomass, there are multiple internal
446 factors, such as species, physiological characteristics, and plant hydraulics, that would affect vegetation
447 productivity. Because of that, we believe that agricultural drought, referring to the drought that impacts
448 vegetation productivity, is the most proper term, as originally defined by [Wilhite and Glantz \(1985\)](#).

449 The study results showed that the soil moisture-based drought index (SSI) was better at explaining vegeta-
450 tion productivity across land cover macroclasses than meteorological drought indices like SPI, SPEI, and
451 EDDI. In the early growing season and especially in irrigated rather than rainfed croplands, soil moisture
452 has better skills than SPI and SPEI for estimating gross primary production (GPP). This according to
453 [Chatterjee et al. \(2022\)](#) evaluation of the SPI and SPEI and their correlation with GPP in the CONUS.
454 Also, [Zhou et al. \(2021\)](#) indicate that the monthly scaled Standardized Water Deficit Index (SWDI) can
455 accurately show the effects of agricultural drought in most of China. [Nicolai-Shaw et al. \(2017\)](#) also looked
456 at the time-lag between the SWDI and the Vegetation Condition Index (VCI). They found that there was
457 little to no time-lag in croplands but a greater time-lag in forests.

458 In our case, there is strong spatial variability throughout Chile and between classes, mainly attributable to
459 climate heterogeneity, hydrological status, or vegetation resistance to water scarcity. The semi-arid “Norte
460 Chico” and the Mediterranean “Centro” were where SSI had the best performance. In Chile, medium-term
461 deficits of 12 months are more relevant in the response of vegetation, which decreases to the south, and in the
462 case of croplands, they seem to react in a shorter time, with six months (SSI-6) in “Centro.” This variation
463 for croplands could be related to the fact that in “Norte Chico,” the majority of crops are irrigated, but
464 to the south there is a higher proportion of rainfed agriculture, which is most dependent on the short-term
465 availability of water. Rather, in the “Norte Chico,” the orchards are more dependent on the storage of water
466 in dams of groundwater reservoirs, which are affected by long-term drought (e.g., SPI-36).

467 *6.4. Future outlook (to complete)*

468 **7. Conclusion**

469 There is a trend toward decreasing water supply in most parts of Chile, particularly in the “Centro” and
470 “Norte Chico” regions. The whole country showed an increase in AED. Vegetation productivity only showed
471 a decrease in the “Norte Chico” and “Centro,” being highest for shrubland and croplands. Forest is the land
472 cover most resistant to drought, as shown along Chile, and shrubland and cropland are the most sensitive.

473 A soil moisture deficit of 12 months (SSI-12) is highly correlated with vegetation productivity for the land
474 cover classes of shrubland, savannas, croplands, and forest in “Norte Chico” and “Centro.” For the southern

475 part of the country with humid conditions, the correlation with SSI decreases. Soil moisture overcomes
476 the capacity to explain vegetation productivity over the supply and demand drought indices in the entire
477 territory.

478 The variation in vegetation productivity appears to be associated with climate variation rather than an-
479 thropogenic factors (e.g., an increase in water demand by irrigated crops). Even though switching to more
480 demanding crops on the land could increase the impact of drought on vegetation, this would need to be
481 more thoroughly investigated, for instance at the watershed level.

482 The results of this study could help in the development of a robust forecasting system for land cover classes
483 in Chile, helping to improve preparedness for climate change impacts on vegetation.

484 Supplementary material

485 References

- 486 Abramowitz, M., Stegun, I.A., 1968. Handbook of mathematical functions with formulas, graphs, and mathematical tables.
487 volume 55. US Government printing office.
- 488 Aceituno, P., Boisier, J.P., Garreaud, R., Rondanelli, R., Rutllant, J.A., 2021. Climate and Weather in Chile, in: Fernández,
489 B., Gironás, J. (Eds.), Water Resources of Chile. Springer International Publishing, Cham. volume 8, pp. 7–29. URL:
490 http://link.springer.com/10.1007/978-3-030-56901-3_2.
- 491 AghaKouchak, A., Mirchi, A., Madani, K., Di Baldassarre, G., Nazemi, A., Alborzi, A., Anjileli, H., Azarderakhsh, M., Chiang,
492 F., Hassanzadeh, E., Huning, L.S., Mallakpour, I., Martinez, A., Mazdiyasni, O., Moftakhari, H., Norouzi, H., Sadegh,
493 M., Sadeqi, D., Van Loon, A.F., Wanders, N., 2021. Anthropogenic Drought: Definition, Challenges, and Opportuni-
494 ties. *Reviews of Geophysics* 59, e2019RG000683. URL: <https://agupubs.onlinelibrary.wiley.com/doi/10.1029/2019RG000683>, doi:[10.1029/2019RG000683](https://doi.org/10.1029/2019RG000683).
- 495 Akinyemi, F.O., 2021. Vegetation Trends, Drought Severity and Land Use-Land Cover Change during the Growing Season in
496 Semi-Arid Contexts. *Remote Sensing* 2021, Vol. 13, Page 836 13, 836. URL: <https://www.mdpi.com/2072-4292/13/5/836/>
497 htm, doi:[10.3390/RS13050836](https://doi.org/10.3390/RS13050836). publisher: Multidisciplinary Digital Publishing Institute.
- 498 Bakker, K., 2012. Water Security: Research Challenges and Opportunities. *Science* 337, 914–915. URL: <https://www.science.org/doi/10.1126/science.1226337>, doi:[10.1126/science.1226337](https://doi.org/10.1126/science.1226337).
- 499 Beck, H.E., McVicar, T.R., Vergopolan, N., Berg, A., Lutsko, N.J., Dufour, A., Zeng, Z., Jiang, X., van Dijk, A.I.J.M., Miralles,
500 D.G., 2023. High-resolution (1 km) Köppen-Geiger maps for 1901–2099 based on constrained CMIP6 projections. *Scientific
501 Data* 10. URL: <http://dx.doi.org/10.1038/s41597-023-02549-6>, doi:[10.1038/s41597-023-02549-6](https://doi.org/10.1038/s41597-023-02549-6).
- 502 Beguería, S., Vicente-Serrano, S.M., 2023. SPEI: Calculation of the Standardized Precipitation-Evapotranspiration Index. URL:
503 <https://CRAN.R-project.org/package=SPEI>.
- 504 Boisier, J.P., Alvarez-Garreton, C., Cordero, R.R., Damiani, A., Gallardo, L., Garreaud, R.D., Lambert, F., Ramallo, C.,
505 Rojas, M., Rondanelli, R., 2018. Anthropogenic drying in central-southern Chile evidenced by long-term observations
506 and climate model simulations. *Elementa* 6, 74. URL: <https://www.elementascience.org/article/10.1525/elementa.328/>,
507 doi:[10.1525/elementa.328](https://doi.org/10.1525/elementa.328).
- 508 Calvin, K., Dasgupta, D., Krinner, G., Mukherji, A., Thorne, P.W., Trisos, C., Romero, J., Aldunce, P., Barrett, K., Blanco,
509 G., Cheung, W.W., Connors, S., Denton, F., Dioungue-Niang, A., Dodman, D., Garschagen, M., Geden, O., Hayward, B.,
510 Jones, C., Jotzo, F., Krug, T., Lasco, R., Lee, Y.Y., Masson-Delmotte, V., Meinshausen, M., Mintenbeck, K., Mokssit, A.,
511 Otto, F.E., Pathak, M., Pirani, A., Poloczanska, E., Pörtner, H.O., Revi, A., Roberts, D.C., Roy, J., Ruane, A.C., Skea,
512 J., Shukla, P.R., Slade, R., Slangen, A., Sokona, Y., Sörensson, A.A., Tignor, M., Van Vuuren, D., Wei, Y.M., Winkler,
513 H., Zhai, P., Zommers, Z., Hourcade, J.C., Johnson, F.X., Pachauri, S., Simpson, N.P., Singh, C., Thomas, A., Totin, E.,
514 Arias, P., Bustamante, M., Elgizouli, I., Flato, G., Howden, M., Méndez-Vallejo, C., Pereira, J.J., Pichs-Madruga, R., Rose,
515 S.K., Saheb, Y., Sánchez Rodríguez, R., Ürge Vorsatz, D., Xiao, C., Yassa, N., Alegria, A., Armour, K., Bednar-Friedl, B.,
516 Blok, K., Cissé, G., Dentener, F., Eriksen, S., Fischer, E., Garner, G., Guiavarch, C., Haasnoot, M., Hansen, G., Hauser, M.,
517 Hawkins, E., Hermans, T., Kopp, R., Leprince-Ringuet, N., Lewis, J., Ley, D., Ludden, C., Niamir, L., Nicholls, Z., Some,
518 S., Szopa, S., Trewin, B., Van Der Wijst, K.I., Winter, G., Witting, M., Birt, A., Ha, M., Romero, J., Kim, J., Haites, E.F.,
519 Jung, Y., Stavins, R., Birt, A., Ha, M., Orendain, D.J.A., Ignon, L., Park, S., Park, Y., Reisinger, A., Cammarano, D.,
520 Fischlin, A., Fuglestvedt, J.S., Hansen, G., Ludden, C., Masson-Delmotte, V., Matthews, J.R., Mintenbeck, K., Pirani, A.,
521 Poloczanska, E., Leprince-Ringuet, N., Péan, C., 2023. IPCC, 2023: Climate Change 2023: Synthesis Report. Contribution
522 of Working Groups I, II and III to the Sixth Assessment Report of the Intergovernmental Panel on Climate Change [Core
523 Writing Team, H. Lee and J. Romero (eds.)]. IPCC, Geneva, Switzerland. Technical Report. Intergovernmental Panel on
524 Climate Change (IPCC). URL: <https://www.ipcc.ch/report/ar6/syr/>.
- 525 Chamling, M., Bera, B., 2020. Spatio-temporal Patterns of Land Use/Land Cover Change in the Bhutan–Bengal Foothill Region
526 Between 1987 and 2019: Study Towards Geospatial Applications and Policy Making. *Earth Systems and Environment* 4,
527 117–130. URL: <http://link.springer.com/10.1007/s41748-020-00150-0>, doi:[10.1007/s41748-020-00150-0](https://doi.org/10.1007/s41748-020-00150-0).
- 528 Chatterjee, S., Desai, A.R., Zhu, J., Townsend, P.A., Huang, J., 2022. Soil moisture as an essential component for delineating
529 and forecasting agricultural rather than meteorological drought. *Remote Sensing of Environment* 269, 112833. URL: <https://linkinghub.elsevier.com/retrieve/pii/S0034425721005538>, doi:[10.1016/j.rse.2021.112833](https://doi.org/10.1016/j.rse.2021.112833).

- 533 Chen, J., Shao, Z., Huang, X., Zhuang, Q., Dang, C., Cai, B., Zheng, X., Ding, Q., 2022. Assessing the impact of drought-
 534 land cover change on global vegetation greenness and productivity. *Science of The Total Environment* 852, 158499. URL:
 535 <https://linkinghub.elsevier.com/retrieve/pii/S004896972205598X>, doi:10.1016/j.scitotenv.2022.158499.
- 536 Crausbay, S.D., Ramirez, A.R., Carter, S.L., Cross, M.S., Hall, K.R., Bathke, D.J., Betancourt, J.L., Colt, S., Cravens, A.E.,
 537 Dalton, M.S., Dunham, J.B., Hay, L.E., Hayes, M.J., McEvoy, J., McNutt, C.A., Moritz, M.A., Nislow, K.H., Raheem, N.,
 538 Sanford, T., 2017. Defining Ecological Drought for the Twenty-First Century. *Bulletin of the American Meteorological Society*
 539 98, 2543–2550. URL: <https://journals.ametsoc.org/view/journals/bams/98/12/bams-d-16-0292.1.xml>, doi:10.1175/BAMS-D-
 540 16-0292.1. publisher: American Meteorological Society.
- 541 Dai, M., Huang, S., Huang, Q., Leng, G., Guo, Y., Wang, L., Fang, W., Li, P., Zheng, X., 2020. Assessing agricultural drought
 542 risk and its dynamic evolution characteristics. *Agricultural Water Management* 231, 106003. URL: <https://linkinghub.elsevier.com/retrieve/pii/S0378377419316531>, doi:10.1016/j.agwat.2020.106003.
- 543 Didan, K., 2015. MOD13Q1 MODIS/Terra Vegetation Indices 16-Day L3 Global 250m SIN Grid V006. Technical Report.
 544 NASA EOSDIS Land Processes DAAC. doi:<http://dx.doi.org/10.5067/MODIS/MOD13Q1.006>.
- 545 Farahmand, A., AghaKouchak, A., 2015. A generalized framework for deriving nonparametric standardized drought indicators.
 546 *Advances in Water Resources* 76, 140–145. URL: <https://linkinghub.elsevier.com/retrieve/pii/S0309170814002322>, doi:10.
 547 1016/j.advwatres.2014.11.012.
- 548 Fathi-Taperasht, A., Shafizadeh-Moghadam, H., Minaei, M., Xu, T., 2022. Influence of drought duration and severity on
 549 drought recovery period for different land cover types: evaluation using MODIS-based indices. *Ecological Indicators* 141,
 550 109146. URL: <https://linkinghub.elsevier.com/retrieve/pii/S1470160X22006185>, doi:10.1016/j.ecolind.2022.109146.
- 551 Friedl, M., Sulla-Menashe, D., 2019. MCD12Q1 MODIS/Terra+Aqua Land Cover Type Yearly L3 Global 500m SIN Grid V006
 552 [Data set]. NASA EOSDIS Land Processes DAAC. doi:[10.5067/MODIS/MCD12Q1.006](http://dx.doi.org/10.5067/MODIS/MCD12Q1.006).
- 553 Fuentes, I., Fuster, R., Avilés, D., Vervoort, W., 2021. Water scarcity in central Chile: the effect of climate and land cover
 554 changes on hydrologic resources. *Hydrological Sciences Journal* 66, 1028–1044. URL: <https://www.tandfonline.com/doi/full/10.1080/02626667.2021.1903475>, doi:10.1080/02626667.2021.1903475.
- 555 Garreaud, R., Alvarez-Garreton, C., Barichivich, J., Boisier, J.P., Christie, D., Galleguillos, M., LeQuenne, C., McPhee, J.,
 556 Zambrano-Bigiarini, M., 2017. The 2010–2015 mega drought in Central Chile: Impacts on regional hydroclimate and
 557 vegetation. *Hydrology and Earth System Sciences Discussions* 2017, 1–37. URL: <http://www.hydrol-earth-syst-sci-discuss.net/hess-2017-191/>, doi:10.5194/hess-2017-191.
- 558 Garreaud, R.D., 2009. The Andes climate and weather. *Advances in Geosciences* 22, 3–11. URL: <https://adgeo.copernicus.org/articles/22/3/2009/>, doi:10.5194/adgeo-22-3-2009.
- 559 Hargreaves, G.H., 1994. Defining and Using Reference Evapotranspiration. *Journal of Irrigation and Drainage Engineering* 120,
 560 1132–1139. URL: <https://ascelibrary.org/doi/10.1061/%28ASCE%290733-9437%281994%29120%3A6%281132%29>, doi:10.
 561 1061/(ASCE)0733-9437(1994)120:6(1132).
- 562 Hargreaves, G.H., Samani, Z.A., 1985. Reference crop evapotranspiration from temperature. *Applied engineering in agriculture*
 563 1, 96–99.
- 564 Heim, R.R., 2002. A Review of Twentieth-Century Drought Indices Used in the United States. *Bulletin of the American
 565 Meteorological Society* 83, 1149–1166. URL: <https://journals.ametsoc.org/doi/10.1175/1520-0477-83.8.1149>, doi:10.1175/
 566 1520-0477-83.8.1149.
- 567 Hijmans, R.J., 2023. terra: Spatial Data Analysis. URL: <https://CRAN.R-project.org/package=terra>.
- 568 Ho, T.K., 1995. Random decision forests, in: *Proceedings of 3rd international conference on document analysis and recognition*,
 569 IEEE. pp. 278–282.
- 570 Hobbins, M.T., Wood, A., McEvoy, D.J., Huntington, J.L., Morton, C., Anderson, M., Hain, C., 2016. The Evaporative Demand
 571 Drought Index. Part I: Linking Drought Evolution to Variations in Evaporative Demand. *Journal of Hydrometeorology* 17,
 572 1745–1761. URL: <https://journals.ametsoc.org/doi/10.1175/JHM-D-15-0121.1>, doi:10.1175/JHM-D-15-0121.1.
- 573 Homer, C., Dewitz, J., Jin, S., Xian, G., Costello, C., Danielson, P., Gass, L., Funk, M., Wickham, J., Stehman, S., Auch, R.,
 574 Riitters, K., 2020. Conterminous United States land cover change patterns 2001–2016 from the 2016 National Land Cover
 575 Database. *ISPRS Journal of Photogrammetry and Remote Sensing* 162, 184–199. URL: <https://linkinghub.elsevier.com/retrieve/pii/S0924271620300587>, doi:10.1016/j.isprsjprs.2020.02.019.
- 576 Hufkens, K., Stauffer, R., Campitelli, E., 2019. The ecwmfr package: an interface to ECMWF API endpoints. URL: <https://bluegreen-labs.github.io/ecwmfr/>.
- 577 Humphrey, V., Berg, A., Ciais, P., Gentine, P., Jung, M., Reichstein, M., Seneviratne, S.I., Frankenberg, C., 2021. Soil
 578 moisture–atmosphere feedback dominates land carbon uptake variability. *Nature* 592, 65–69. URL: <https://www.nature.com/articles/s41586-021-03325-5>, doi:10.1038/s41586-021-03325-5.
- 579 IPCC, 2013. Climate Change 2013: The Physical Science Basis. Contribution of Working Group I to the Fifth Assessment
 580 Report of the Intergovernmental Panel on Climate Change. Cambridge University Press, Cambridge, UK; New York, USA.
 581 URL: www.climatechange2013.org, doi:10.1017/CBO9781107415324.
- 582 Jiang, W., Wang, L., Feng, L., Zhang, M., Yao, R., 2020. Drought characteristics and its impact on changes in surface
 583 vegetation from 1981 to 2015 in the Yangtze River Basin, China. *International Journal of Climatology* 40, 3380–3397. URL:
 584 <https://rmets.onlinelibrary.wiley.com/doi/10.1002/joc.6403>, doi:10.1002/joc.6403.
- 585 Kendall, M., 1975. Rank correlation methods (4th ed. 2d impression). Griffin.
- 586 Kogan, F., Guo, W., Yang, W., 2020. Near 40-year drought trend during 1981–2019 earth warming and food security. *Geomatics,
 587 Natural Hazards and Risk* 11, 469–490. URL: <https://www.tandfonline.com/doi/full/10.1080/19475705.2020.1730452>, doi:10.1080/19475705.2020.1730452.
- 588 Laimighofer, J., Laaha, G., 2022. How standard are standardized drought indices? Uncertainty components for the SPI
 589 & SPEI case. *Journal of Hydrology* 613, 128385. URL: <https://linkinghub.elsevier.com/retrieve/pii/S0022169422009544>,

- 598 doi:[10.1016/j.jhydrol.2022.128385](https://doi.org/10.1016/j.jhydrol.2022.128385).
- 599 Li, W., Migliavacca, M., Forkel, M., Denissen, J.M.C., Reichstein, M., Yang, H., Duveiller, G., Weber, U., Orth, R., 2022.
600 Widespread increasing vegetation sensitivity to soil moisture. *Nature Communications* 13, 3959. URL: <https://www.nature.com/articles/s41467-022-31667-9>, doi:[10.1038/s41467-022-31667-9](https://doi.org/10.1038/s41467-022-31667-9).
- 601 Luebert, F., Pliscoff, P., 2022. The vegetation of Chile and the EcoVeg approach in the context of the International Vegetation
602 Classification project. *Vegetation Classification and Survey* 3, 15–28. URL: <https://vcs.pensoft.net/article/67893/>, doi:[10.3897/VCS.67893](https://doi.org/10.3897/VCS.67893).
- 603 Luyssaert, S., Jammet, M., Stoy, P.C., Estel, S., Pongratz, J., Ceschia, E., Churkina, G., Don, A., Erb, K., Ferlicoq, M.,
604 Gielen, B., Grünwald, T., Houghton, R.A., Klumpp, K., Knohl, A., Kolb, T., Kuemmerle, T., Laurila, T., Lohila, A.,
605 Loustau, D., McGrath, M.J., Meyfroidt, P., Moors, E.J., Naudts, K., Novick, K., Otto, J., Pilegaard, K., Pio, C.A., Rambal,
606 S., Rebmann, C., Ryder, J., Suyker, A.E., Varlagin, A., Wattenbach, M., Dolman, A.J., 2014. Land management and
607 land-cover change have impacts of similar magnitude on surface temperature. *Nature Climate Change* 4, 389–393. URL:
608 <https://www.nature.com/articles/nclimate2196>, doi:[10.1038/nclimate2196](https://doi.org/10.1038/nclimate2196).
- 609 Masson-Delmotte, V., P.Z.A.P.S.L.C.C.P.S.B.N.C.Y.C.L.G.M.I.G.M.H.K.L.E.L.J.B.R.M.T.K.M.T.W.O.Y.R.Y.a.B.Z.e., 2021.
610 IPCC, 2021: Climate Change 2021: The Physical Science Basis. Contribution of Working Group I to the Sixth Assessment
611 Report of the Intergovernmental Panel on Climate Change. Technical Report. URL: <https://www.ipcc.ch/>. publication
612 Title: Cambridge University Press. In Press.
- 613 McEvoy, D.J., Huntington, J.L., Hobbins, M.T., Wood, A., Morton, C., Anderson, M., Hain, C., 2016. The Evaporative Demand
614 Drought Index. Part II: CONUS-Wide Assessment against Common Drought Indicators. *Journal of Hydrometeorology* 17,
615 1763–1779. URL: <http://journals.ametsoc.org/doi/10.1175/JHM-D-15-0122.1>, doi:[10.1175/JHM-D-15-0122.1](https://doi.org/10.1175/JHM-D-15-0122.1).
- 616 Meroni, M., Rembold, F., Fasbender, D., Vrieling, A., 2017. Evaluation of the Standardized Precipitation Index as an early
617 predictor of seasonal vegetation production anomalies in the Sahel. *Remote Sensing Letters* 8, 301–310. URL: <http://www.tandfonline.com/doi/abs/10.1080/2150704X.2016.1264020>, doi:[10.1080/2150704X.2016.1264020](https://doi.org/10.1080/2150704X.2016.1264020).
- 618 Miranda, A., Lara, A., Altamirano, A., Di Bella, C., González, M.E., Julio Camarero, J., 2020. Forest browning trends in
619 response to drought in a highly threatened mediterranean landscape of South America. *Ecological Indicators* 115, 106401.
620 URL: <https://linkinghub.elsevier.com/retrieve/pii/S1470160X20303381>, doi:[10.1016/j.ecolind.2020.106401](https://doi.org/10.1016/j.ecolind.2020.106401).
- 621 Miranda, A., Syphard, A.D., Berdugo, M., Carrasco, J., Gómez-González, S., Ovalle, J.F., Delpiano, C.A., Vargas, S.,
622 Squeo, F.A., Miranda, M.D., Dobbs, C., Mentler, R., Lara, A., Garreaud, R., 2023. Widespread synchronous decline
623 of Mediterranean-type forest driven by accelerated aridity. *Nature Plants* 9, 1810–1817. URL: <https://www.nature.com/articles/s41477-023-01541-7>, doi:[10.1038/s41477-023-01541-7](https://doi.org/10.1038/s41477-023-01541-7).
- 624 Muñoz-Sabater, J., Dutra, E., Agustí-Panareda, A., Albergel, C., Arduini, G., Balsamo, G., Boussetta, S., Choulga, M.,
625 Harrigan, S., Hersbach, H., Martens, B., Miralles, D.G., Piles, M., Rodríguez-Fernández, N.J., Zsoter, E., Buontempo, C.,
626 Thépaut, J.N., 2021. ERA5-Land: a state-of-the-art global reanalysis dataset for land applications. *Earth System Science
627 Data* 13, 4349–4383. URL: <https://essd.copernicus.org/articles/13/4349/2021/>, doi:[10.5194/essd-13-4349-2021](https://doi.org/10.5194/essd-13-4349-2021).
- 628 Nicolai-Shaw, N., Zscheischler, J., Hirschi, M., Gudmundsson, L., Seneviratne, S.I., 2017. A drought event composite analysis
629 using satellite remote-sensing based soil moisture. *Remote Sensing of Environment* 203, 216–225. URL: <https://linkinghub.elsevier.com/retrieve/pii/S0034425717302729>, doi:[10.1016/j.rse.2017.06.014](https://doi.org/10.1016/j.rse.2017.06.014).
- 630 Noguera, I., Vicente-Serrano, S.M., Domínguez-Castro, F., 2022. The Rise of Atmospheric Evaporative Demand Is Increasing
631 Flash Droughts in Spain During the Warm Season. *Geophysical Research Letters* 49, e2021GL097703. URL: <https://agupubs.onlinelibrary.wiley.com/doi/10.1029/2021GL097703>, doi:[10.1029/2021GL097703](https://doi.org/10.1029/2021GL097703).
- 632 Pebesma, E., 2018. Simple Features for R: Standardized Support for Spatial Vector Data. *The R Journal* 10, 439–446. URL:
633 <https://doi.org/10.32614/RJ-2018-009>, doi:[10.32614/RJ-2018-009](https://doi.org/10.32614/RJ-2018-009).
- 634 Pebesma, E., Bivand, R., 2023. Spatial Data Science: With applications in R. Chapman and Hall/CRC, London. URL:
635 <https://r-spatial.org/book/>.
- 636 Peng, D., Zhang, B., Wu, C., Huete, A.R., Gonsamo, A., Lei, L., Ponce-Campos, G.E., Liu, X., Wu, Y., 2017. Country-level
637 net primary production distribution and response to drought and land cover change. *Science of The Total Environment* 574,
638 65–77. URL: <https://linkinghub.elsevier.com/retrieve/pii/S0048969716319507>, doi:[10.1016/j.scitotenv.2016.09.033](https://doi.org/10.1016/j.scitotenv.2016.09.033).
- 639 Pitman, A.J., De Noblet-Ducoudré, N., Avila, F.B., Alexander, L.V., Boisier, J.P., Brovkin, V., Delire, C., Cruz, F., Donat,
640 M.G., Gayler, V., Van Den Hurk, B., Reick, C., Volodko, A., 2012. Effects of land cover change on temperature and
641 rainfall extremes in multi-model ensemble simulations. *Earth System Dynamics* 3, 213–231. URL: <https://esd.copernicus.org/articles/3/213/2012/>, doi:[10.5194/esd-3-213-2012](https://doi.org/10.5194/esd-3-213-2012).
- 642 Potopová, V., Stepánek, P., Mozný, M., Türkott, L., Soukup, J., 2015. Performance of the standarised precipitation evapotranspiration
643 index at various lags for agricultural drought risk assessment in the {C}zech {R}epublic. *Agricultural and Forest Meteorology* 202, 26–38.
- 644 R Core Team, 2023. R: A Language and Environment for Statistical Computing. R Foundation for Statistical Computing,
645 Vienna, Austria. URL: <https://www.R-project.org/>.
- 646 Rhee, J., Im, J., Carbone, G.J., 2010. Monitoring agricultural drought for arid and humid regions using multi-sensor remote
647 sensing data. *Remote Sensing of Environment* 114, 2875–2887. URL: <http://www.sciencedirect.com/science/article/pii/S003442571000221X>, doi:[10.1016/j.rse.2010.07.005](https://doi.org/10.1016/j.rse.2010.07.005).
- 648 Samaniego, L., Thober, S., Kumar, R., Wanders, N., Rakovec, O., Pan, M., Zink, M., Sheffield, J., Wood, E.F., Marx, A.,
649 2018. Anthropogenic warming exacerbates European soil moisture droughts. *Nature Climate Change* 8, 421–426. URL:
650 <https://www.nature.com/articles/s41558-018-0138-5>, doi:[10.1038/s41558-018-0138-5](https://doi.org/10.1038/s41558-018-0138-5).
- 651 Sen, P.K., 1968. Estimates of the Regression Coefficient Based on Kendall's Tau. *Journal of the American Statistical Association*
652 63, 1379–1389. URL: <http://www.tandfonline.com/doi/abs/10.1080/01621459.1968.10480934>, doi:[10.1080/01621459.1968.10480934](https://doi.org/10.1080/01621459.1968.10480934).

- 663 Senf, C., Buras, A., Zang, C.S., Rammig, A., Seidl, R., 2020. Excess forest mortality is consistently linked to drought
 664 across Europe. *Nature Communications* 11, 6200. URL: <https://www.nature.com/articles/s41467-020-19924-1>, doi:[10.1038/s41467-020-19924-1](https://doi.org/10.1038/s41467-020-19924-1).
- 665 Slette, I.J., Post, A.K., Awad, M., Even, T., Punzalan, A., Williams, S., Smith, M.D., Knapp, A.K., 2019. How ecologists
 666 define drought, and why we should do better. *Global Change Biology* 25, 3193–3200. URL: <https://onlinelibrary.wiley.com/doi/10.1111/gcb.14747>, doi:[10.1111/gcb.14747](https://doi.org/10.1111/gcb.14747).
- 667 Song, X.P., Hansen, M.C., Stehman, S.V., Potapov, P.V., Tyukavina, A., Vermote, E.F., Townshend, J.R., 2018. Global land
 668 change from 1982 to 2016. *Nature* 560, 639–643. URL: <https://www.nature.com/articles/s41586-018-0411-9>, doi:[10.1038/s41586-018-0411-9](https://doi.org/10.1038/s41586-018-0411-9).
- 669 Taucare, M., Viguier, B., Figueroa, R., Daniele, L., 2024. The alarming state of Central Chile's groundwater resources: A
 670 paradigmatic case of a lasting overexploitation. *Science of The Total Environment* 906, 167723. URL: <https://linkinghub.elsevier.com/retrieve/pii/S0048969723063507>, doi:[10.1016/j.scitotenv.2023.167723](https://doi.org/10.1016/j.scitotenv.2023.167723).
- 671 Tennekes, M., 2018. tmap: Thematic Maps in R. *Journal of Statistical Software* 84, 1–39. doi:[10.18637/jss.v084.i06](https://doi.org/10.18637/jss.v084.i06).
- 672 Urrutia-Jalabert, R., González, M.E., González-Reyes, ., Lara, A., Garreaud, R., 2018. Climate variability and forest fires in
 673 central and south-central Chile. *Ecosphere* 9, e02171. URL: <https://esajournals.onlinelibrary.wiley.com/doi/10.1002/ecs2.2171>, doi:[10.1002/ecs2.2171](https://doi.org/10.1002/ecs2.2171).
- 674 Van Loon, A.F., Gleeson, T., Clark, J., Van Dijk, A.I., Stahl, K., Hannaford, J., Di Baldassarre, G., Teuling, A.J., Tallaksen,
 675 L.M., Uijlenhoet, R., Hannah, D.M., Sheffield, J., Svoboda, M., Verbeiren, B., Wagener, T., Rangecroft, S., Wanders, N.,
 676 Van Lanen, H.A., 2016. Drought in the Anthropocene. *Nature Geoscience* 9, 89–91. doi:[10.1038/ngeo2646](https://doi.org/10.1038/ngeo2646).
- 677 Venegas-González, A., Juñent, F.R., Gutiérrez, A.G., Filho, M.T., 2018. Recent radial growth decline in response to increased
 678 drought conditions in the northernmost Nothofagus populations from South America. *Forest Ecology and Management* 409,
 679 94–104. URL: <https://linkinghub.elsevier.com/retrieve/pii/S0378112717313993>, doi:[10.1016/j.foreco.2017.11.006](https://doi.org/10.1016/j.foreco.2017.11.006).
- 680 Venegas-González, A., Muñoz, A.A., Carpintero-Gibson, S., González-Reyes, A., Schneider, I., Gipolou-Zúñiga, T., Aguilera-Betti,
 681 I., Roig, F.A., 2023. Sclerophyllous Forest Tree Growth Under the Influence of a Historic Megadrought in the
 682 Mediterranean Ecoregion of Chile. *Ecosystems* 26, 344–361. URL: <https://link.springer.com/10.1007/s10021-022-00760-x>, doi:[10.1007/s10021-022-00760-x](https://doi.org/10.1007/s10021-022-00760-x).
- 683 Vicente-Serrano, S.M., Azorin-Molina, C., Sanchez-Lorenzo, A., Revuelto, J., López-Moreno, J.I., González-Hidalgo, J.C.,
 684 Moran-Tejeda, E., Espejo, F., 2014. Reference evapotranspiration variability and trends in Spain, 1961–2011. *Global
 685 and Planetary Change* 121, 26–40. URL: <https://linkinghub.elsevier.com/retrieve/pii/S0921818114001180>, doi:[10.1016/j.gloplacha.2014.06.005](https://doi.org/10.1016/j.gloplacha.2014.06.005).
- 686 Vicente-Serrano, S.M., Beguería, S., López-Moreno, J.I., 2010. A multiscalar drought index sensitive to global warming: The
 687 standardized precipitation evapotranspiration index. *Journal of Climate* 23, 1696–1718. URL: <http://dx.doi.org/10.1175/2009JCLI2909.1>, doi:[10.1175/2009JCLI2909.1](https://doi.org/10.1175/2009JCLI2909.1).
- 688 Vicente-Serrano, S.M., Peña-Angulo, D., Beguería, S., Domínguez-Castro, F., Tomás-Burguera, M., Noguera, I., Gimeno-Sotelo,
 689 L., El Kenawy, A., 2022. Global drought trends and future projections. *Philosophical Transactions of the Royal Society A:
 690 Mathematical, Physical and Engineering Sciences* 380, 20210285. URL: <https://royalsocietypublishing.org/doi/10.1098/rsta.2021.0285>, doi:[10.1098/rsta.2021.0285](https://doi.org/10.1098/rsta.2021.0285).
- 691 Vicente-Serrano, S.M., McVicar, T.R., Miralles, D.G., Yang, Y., Tomas-Burguera, M., 2020. Unraveling the influence of
 692 atmospheric evaporative demand on drought and its response to climate change. *WIREs Climate Change* 11, e632. URL:
 693 <https://wires.onlinelibrary.wiley.com/doi/10.1002/wcc.632>, doi:[10.1002/wcc.632](https://doi.org/10.1002/wcc.632).
- 694 Wickham, H., Averick, M., Bryan, J., Chang, W., McGowan, L.D., François, R., Grolemund, G., Hayes, A., Henry, L., Hester,
 695 J., Kuhn, M., Pedersen, T.L., Miller, E., Bache, S.M., Müller, K., Ooms, J., Robinson, D., Seidel, D.P., Spinu, V., Takahashi,
 696 K., Vaughan, D., Wilke, C., Woo, K., Yutani, H., 2019. Welcome to the tidyverse. *Journal of Open Source Software* 4, 1686.
 697 doi:[10.21105/joss.01686](https://doi.org/10.21105/joss.01686).
- 698 Wilhite, D.A., Glantz, M.H., 1985. Understanding: The drought phenomenon: The role of definitions. *Water International* 10,
 699 111–120. URL: <http://dx.doi.org/10.1080/02508068508686328>, doi:[10.1080/02508068508686328](https://doi.org/10.1080/02508068508686328).
- 700 Wilks, D.S., 2011. Empirical distributions and exploratory data analysis. *Statistical Methods in the Atmospheric Sciences* 100.
- 701 Winkler, K., Fuchs, R., Rounsevell, M., Herold, M., 2021. Global land use changes are four times greater than previously
 702 estimated. *Nature Communications* 12, 2501. URL: <https://www.nature.com/articles/s41467-021-22702-2>, doi:[10.1038/s41467-021-22702-2](https://doi.org/10.1038/s41467-021-22702-2).
- 703 Wu, C., Zhong, L., Yeh, P.J.F., Gong, Z., Lv, W., Chen, B., Zhou, J., Li, J., Wang, S., 2024. An evaluation framework
 704 for quantifying vegetation loss and recovery in response to meteorological drought based on SPEI and NDVI. *Science of
 705 The Total Environment* 906, 167632. URL: <https://linkinghub.elsevier.com/retrieve/pii/S0048969723062599>, doi:[10.1016/j.scitotenv.2023.167632](https://doi.org/10.1016/j.scitotenv.2023.167632).
- 706 Xiao, C., Zaehle, S., Yang, H., Wigneron, J.P., Schmullius, C., Bastos, A., 2023. Land cover and management effects on
 707 ecosystem resistance to drought stress. *Earth System Dynamics* 14, 1211–1237. URL: <https://esd.copernicus.org/articles/14/1211/2023/>, doi:[10.5194/esd-14-1211-2023](https://doi.org/10.5194/esd-14-1211-2023).
- 708 Yang, J., Huang, X., 2021. The 30 m annual land cover dataset and its dynamics in China from 1990 to 2019. *Earth System
 709 Science Data* 13, 3907–3925. URL: <https://essd.copernicus.org/articles/13/3907/2021/>, doi:[10.5194/essd-13-3907-2021](https://doi.org/10.5194/essd-13-3907-2021).
- 710 Zambrano, F., 2023. Four decades of satellite data for agricultural drought monitoring throughout the growing season in Central
 711 Chile, in: Vijay P. Singh Deepak Jhajharia, R.M., Kumar, R. (Eds.), *Integrated Drought Management*, Two Volume Set.
 712 CRC Press, p. 28.
- 713 Zambrano, F., Lillo-Saavedra, M., Verbist, K., Lagos, O., 2016. Sixteen years of agricultural drought assessment of the
 714 biobío region in chile using a 250 m resolution vegetation condition index (VCI). *Remote Sensing* 8, 1–20. URL: <http://www.mdpi.com/2072-4292/8/6/530>, doi:[10.3390/rs8060530](https://doi.org/10.3390/rs8060530). publisher: Multidisciplinary Digital Publishing Institute.

- 728 Zambrano, F., Vrieling, A., Nelson, A., Meroni, M., Tadesse, T., 2018. Prediction of drought-induced reduction of agricultural
729 productivity in Chile from MODIS, rainfall estimates, and climate oscillation indices. *Remote Sensing of Environment*
730 219, 15–30. URL: <https://www.sciencedirect.com/science/article/pii/S0034425718304541>, doi:[10.1016/j.rse.2018.10.006](https://doi.org/10.1016/j.rse.2018.10.006).
731 publisher: Elsevier.
- 732 Zambrano, F., Wardlow, B., Tadesse, T., Lillo-Saavedra, M., Lagos, O., 2017. Evaluating satellite-derived long-term historical
733 precipitation datasets for drought monitoring in Chile. *Atmospheric Research* 186, 26–42. URL: <https://www.sciencedirect.com/science/article/pii/S0169809516305865>, doi:[10.1016/j.atmosres.2016.11.006](https://doi.org/10.1016/j.atmosres.2016.11.006). publisher: Elsevier.
- 733 Zhang, W., Wei, F., Horion, S., Fensholt, R., Forkel, M., Brandt, M., 2022. Global quantification of the bidirectional de-
734 pendency between soil moisture and vegetation productivity. *Agricultural and Forest Meteorology* 313, 108735. URL:
735 <https://linkinghub.elsevier.com/retrieve/pii/S0168192321004214>, doi:[10.1016/j.agrformet.2021.108735](https://doi.org/10.1016/j.agrformet.2021.108735).
- 736 Zhao, Y., Feng, D., Yu, L., Wang, X., Chen, Y., Bai, Y., Hernández, H.J., Galleguillos, M., Estades, C., Biging, G.S., Radke,
737 J.D., Gong, P., 2016. Detailed dynamic land cover mapping of Chile: Accuracy improvement by integrating multi-temporal
738 data. *Remote Sensing of Environment* 183, 170–185. URL: <https://linkinghub.elsevier.com/retrieve/pii/S0034425716302188>,
739 doi:[10.1016/j.rse.2016.05.016](https://doi.org/10.1016/j.rse.2016.05.016).
- 740 Zhou, K., Li, J., Zhang, T., Kang, A., 2021. The use of combined soil moisture data to characterize agricultural drought
741 conditions and the relationship among different drought types in China. *Agricultural Water Management* 243, 106479. URL:
742 <https://linkinghub.elsevier.com/retrieve/pii/S0378377420305965>, doi:[10.1016/j.agwat.2020.106479](https://doi.org/10.1016/j.agwat.2020.106479).
- 743
- 744